6-2018

Toward Controllable Hydraulic Coupling of Joints in a Wearable Robot

Emma Treadway
etreadwa@trinity.edu

Z. Gan

C. D. Remy

R. Brent Gillespie

HHS Public Access

Author manuscript

IEEE Trans Robot. Author manuscript; available in PMC 2019 June 01.

Published in final edited form as:

IEEE Trans Robot. 2018 June ; 34(3): 748–763. doi:10.1109/TRO.2018.2799597.

Toward Controllable Hydraulic Coupling of Joints in a Wearable Robot

Emma Treadway, Student Member, IEEE, **Zhenyu Gan**, **C. David Remy, Member, IEEE**, and **R. Brent Gillespie, Member, IEEE**

Department of Mechanical Engineering, University of Michigan, Ann Arbor, MI, 48109 USA

Abstract

In this paper, we develop theoretical foundations for a new class of rehabilitation robot: body powered devices that route power between a user's joints. By harvesting power from a healthy joint to assist an impaired joint, novel bimanual and self-assist therapies are enabled. This approach complements existing robotic therapies aimed at promoting recovery of motor function after neurological injury.

We employ hydraulic transmissions for routing power, or equivalently for coupling the motions of a user's joints. Fluid power routed through flexible tubing imposes constraints within a limb or between homologous joints across the body. Variable transmissions allow constraints to be steered on the fly, and simple valve switching realizes free space and locked motion.

We examine two methods for realizing variable hydraulic transmissions: using valves to switch among redundant cylinders (digital hydraulics) or using an intervening electromechanical link. For both methods, we present a rigorous mathematical framework for describing and controlling the resulting constraints. Theoretical developments are supported by experiments using a prototype fluid-power exoskeleton.

Index Terms

Physical Human-Robot Interaction; Rehabilitation Robotics; Cooperative Manipulators; Cobots; Haptics and Haptic Interfaces

I. Introduction

ROBOTIC solutions will soon become available for delivering physical therapy to patients who have suffered a neurological injury such as stroke or spinal cord injury. Approaches include mechanizing conventional therapies in which a therapist provides movement assistance to a patient [1], engaging motor adaptation and aftereffects through exposure to novel force fields [2], and exercising normative movement patterns against strategically placed or timed loads [3]; more exhaustive lists of approaches can be found in [4], [5]. Robots can offer high dosage with precise, finely adapted therapies in addition to online diagnostic functions to promote recovery of motor function. Typically, rehabilitation robots

are powered by geared motors sufficient to match human torque and must be ground mounted to support their weight [5].

Underexplored for application in rehabilitation robotics are technologies that passively route power from available sources for delivery to the weak or discoordinated limbs of a patient. Routing power to weak joints from stronger ones is equivalent to imposing constraints between them. Cobot technology, used in the field of robotics to impose endpoint motion constraints, offers a possible solution. A cobot is an inherently passive robot intended to collaborate with a human operator by creating motion guides (virtual fixtures) in a shared workspace [6]. Traditionally, the cobot simplifies manual tasks for the human, who can concentrate on regulating speed rather than direction of motion while pushing against the guides. To vary the direction of motion available to the operator, a cobot features continuously variable transmissions (CVTs) but notably lacks drive motors. Jabre et al. [7] and Pan et al. [8] have presented ground-mounted cobots capable of guiding a patient's hand within a workspace. By virtue of inherent passivity, these cobots guarantee safe interaction while guiding patient-generated motion.

Even better for therapy than a ground-mounted cobot interacting with its user through a single end-effector would be a wearable cobot, capable of constraining the manner in which joint motions are coordinated. Examples of wearable cobot designs include [9] and [10]. Such joint constraints could be used to reinforce desirable motion synergies [11] or provide resistance forces when the patient attempts to stray from a constrained manifold. A wearable cobotic exoskeleton that couples joints might span multiple limbs—for example the paretic and nonparetic limbs of a stroke patient—to enable therapy paradigms in which the motions of the limbs are coupled. This would facilitate bimanual therapy by "teaming" healthy joints with impaired joints. Bimanual therapy has been of increasing interest for the potential benefits of task-specific and functional therapy for activities that require the coordination of both hands [12], [13].

Cobot technology in its current state of development cannot support therapies based on self-assist or routing power across the body. The CVTs used to realize cobots are based on steered rolling contacts, whose realizations also tend to be bulky and heavy. The ability to support loads without slipping is directly related to the forces transmitted across the rolling contacts, so the need for high contact forces has led to structurally stronger and correspondingly heavier cobot designs [9], [10], [14]. To truly enable wearability, a lightweight variable transmission technology is needed.

In this paper we explore hydraulic transmissions, since routing fluid power through flexible tubes around the body is simple, accommodates off-axis motions, and provides a high power density transmission. Introducing a hydraulic transmission between two cylinders imposes a constraint on the motions and loads at the two cylinder pistons, since fluid volumes on either side of each piston interact directly with one another across hydraulic lines (yielding common pressure and flow) in an ideal transmission. Fig. 1 shows such a wearable hydraulic exoskeleton prototype that links the motion of the wearer's two elbows.

The ability to modulate the constraint imposed by the transmission would enable the coordination of motions between joints. To coordinate, for example, a strong knee and an impaired ankle, the relationship between the joint angles must be modulated on the fly (while walking). Achieving this flexibility requires the transmission ratio to be variable. We propose to achieve this flexibility in one of two ways: through a hydraulic transformer with variable transmission ratio, or with digital hydraulics [15]–[18] that makes use of valves and sets of multiple cylinders spanning each joint.

In this paper, we introduce hydraulic transmissions as an alternative to rolling-contact CVTs to enable the creation of a new class of cobot-inspired hydraulic exoskeleton. In Section II, we discuss the concepts of virtual surfaces and freespace in our hydraulic joint coupling machines, including our proposed methods for achieving a variable transmission ratio, and we further discuss the ways in which this technology is similar to and different from a rolling transmission cobot. In Section III, we recap and expand the control framework in [19], focusing now on the control of constraints realized with hydraulic transmissions. In Section IV, we develop controllers for a two-axis hydraulic joint coupling exoskeleton designed to be worn on either one or two upper limbs. Sections V and VI provide experimental results to support our theoretical conclusions.

II. Hydraulic Constraints, Virtual Surfaces, and Relation to Cobots

A. Transmissions for Constraints

A simple cobot with a 2-dimensional Cartesian taskspace can be realized using a single wheel rolling against a flat surface. As described in [6], the steering axis of the wheel is held vertical by a linkage or Cartesian frame, and a user grasps this “Unicycle Cobot” by a force-sensing handle configured directly above the wheel contact point (see Fig. 2). The coordinates (x, y) of the contact point become the variables that parameterize the taskspace (and equivalently for this Cartesian example, the jointspace). If the heading of the wheel makes an angle ϕ relative to the x-axis, then a no-slip condition in the lateral direction of the wheel constrains the relative magnitudes of the velocities in the x and y directions: $\dot{y}/\dot{x} = \tan\phi$. The constraint is easily modulated by actively steering the wheel heading as a function of position variables or force applied by the user [6].

This example of a wheel rolling in a Cartesian x-y plane removes a single degree of freedom (DOF) from the cobot, rendering a one-dimensional constraint in a two-dimensional taskspace. More generally, cobots can use multiple wheels, which might roll in the plane, on a sphere [6], or on a drum [14], to restrict more degrees of freedom and remove any number of DOF under program control.

As an alternative to the rolling contact, we propose to impose a constraint among taskspace or jointspace velocities using a hydraulic circuit and set of piston cylinders. Let us begin with an example containing only two piston cylinders: one driving the x-axis and the other driving the y-axis of a Cartesian rail system (Fig. 3). A constraint arises from the conservation of flow in a circuit containing incompressible fluid with no leakage [15]; given the flows Q_1 and Q_2 out of the two cylinders, the relationship $Q_1 + Q_2 = 0$ or

$$Q_2 = -Q_1 \quad (1)$$

is enforced. And given face areas A_1 and A_2 for the pistons driving motion in the x and y axes, respectively, we know that the relationships

$$\dot{x} = -Q_1/A_1, \quad (2)$$

$$\dot{y} = -Q_2/A_2$$

will hold. The flow constraint can thus be converted into a constraint on the x and y velocities of the endpoint:

$$\frac{\dot{y}}{\dot{x}} = -\frac{A_1}{A_2} \quad (3)$$

In general, we could view these relationships as variable ones—we could manipulate either the relationship between the flows in (1) (as with a hydraulic transformer) or the relationship between face areas in (3) to modulate the relationship between the joint velocities.

B. Modulating The Constraint by Hydraulic Circuit Switching

Let us begin with the relationship (3) between face areas. Since a variable-area cylinder is no trivial mechanical achievement, we instead add redundant cylinders and make use of valves to switch certain cylinders in and out of the circuit. Cylinders of various face areas can be arranged in parallel to span the same motion axis, creating a set of effective face areas from which values can be selected by valve switching. Consider a design featuring m single-acting cylinders with flows Q_i out of each cylinder stacked to form the vector $\boldsymbol{Q} = [Q_1, \cdots, Q_m]^T$. And consider a hydraulic manifold with p ports with flows f_i into each port stacked to form the vector $\boldsymbol{f} = [f_1, \cdots, f_p]^T$. A selection matrix $\mathbf{S} \in \Re^{p \times m}$ can then be set up to describe how the m cylinders are connected to the p manifold ports, where valves are introduced into the circuit, and finally whether each valve is open or closed between the manifold port and cylinder. Manifold flows and cylinder flows are then related through

$$\boldsymbol{f} = \mathbf{S}\boldsymbol{Q}. \quad (4)$$

In the following exposition, we use 2-position 3-way valves that are either open between a manifold port and a given cylinder or closed to the manifold port while connecting that cylinder to a common reservoir. Thus a value of 1 in the ith row and jth column of $\mathbf{S}$ indicates that the ith manifold port is connected to the jth cylinder. Since the valves connect

each cylinder to either the reservoir or a single manifold port, each column of **S** has at most a single 1 entry.

Take for example a Cartesian fluid constraint machine with two cylinders driving the x axis and another 2 cylinders driving the y axis, with face areas $A_1, \cdots, A_4$ and flows $Q_1, \cdots, Q_4$. And consider a manifold with 3 ports interconnecting the four cylinders as shown in Fig. 4. The matrix **S** may be defined as follows for this example

$$\mathbf{S} = \begin{bmatrix} S_{11} & 0 & 0 & 0 \\ 0 & S_{22} & 0 & 0 \\ 0 & 0 & S_{33} & S_{34} \end{bmatrix}, \quad (5)$$

where the elements S_{ij} take on values of 0 or 1 depending on the valve settings.

The flow constraint that we formerly characterized in terms of the elements of $\boldsymbol{Q}$ in (1) can now be written in terms of the elements of $\boldsymbol{f}$. If a simple hydraulic manifold is defined as a single fixed volume to which all lines are connected, then conservation of flow of an incompressible fluid imposes a single constraint among the manifold flows. In mathematical terms, the elements of $\boldsymbol{f}$ sum to zero, or

$$\mathbf{C}^T \boldsymbol{f} = 0, \quad (6)$$

where $\boldsymbol{C} = [1, 1, \cdots, 1]^T$. In light of (4), the constraint (1) now reads:

$$\mathbf{C}^T \mathbf{S} \boldsymbol{Q} = \mathbf{0}. \quad (7)$$

This *nonholonomic* constraint will remove one DOF or eliminate one direction of available motion in the cobot workspace.

On the mechanical side of things, the m cylinders (with piston displacements $\boldsymbol{d} = [d_1, \cdots, d_m]^T$) are connected to n joints with configurations $\boldsymbol{q} = [q_1, \cdots, q_n]^T$. A (potentially nonlinear) kinematic function $\boldsymbol{d} = \boldsymbol{h}(\boldsymbol{q})$ maps joint angles to piston extensions. Furthermore, the apparatus acts in a taskspace that may be described by the t taskspace variables $\boldsymbol{R} = [R_1, \cdots, R_t]^T$. We map these to the jointspace variables with the nonlinear forward kinematic function $\boldsymbol{R} = \boldsymbol{g}(\boldsymbol{q})$. For the Cartesian example of Fig. 4, $n = t = 2$ and the jointspace and taskspace variables are equivalent.

Naturally, the cylinder volumes V_i are available by multiplying the piston displacements d_i by the face areas A_i, which may be expressed in matrix form as

$$\boldsymbol{V} = [V_1 V_2 \cdots V_m]^T = \boldsymbol{V_0} - \mathbf{A}\boldsymbol{d}, \quad (8)$$

after collecting the cylinder face areas into the matrix $\mathbf{A} = diag(A_1, \cdots, A_m)$ and the initial volumes into the vector $\boldsymbol{V_0}$. Then we can write

$$\boldsymbol{V} = \boldsymbol{V_0} - \mathbf{A}\boldsymbol{h}(\boldsymbol{q}) = \boldsymbol{V_0} - \mathbf{A}\boldsymbol{h}(\boldsymbol{g}^{-1}(\boldsymbol{R})), \quad (9)$$

The function $\boldsymbol{q} = \boldsymbol{g}^{-1}(\boldsymbol{R})$ describes the inverse kinematics, and will yield recoverable and unique values of $\boldsymbol{q}$ only in non-singular configurations and when no redundancies exist in the kinematic design of the cobot. Typically, kinematic redundancies among joints have been disallowed in cobots [19], and for now we maintain this limitation. Singularities in $\boldsymbol{h}(\boldsymbol{q})$ may be avoided by careful cylinder mounting (for example, as in Fig. 1), and in fact cylinder redundancies which may exist by design pose no problem when cylinders span individual joints. For exoskeletons, singularities in $\boldsymbol{g}^{-1}(\boldsymbol{R})$ can generally be resolved to recover $\boldsymbol{q}$ through the application of the limits imposed by human range-of-motion.

The *holonomic* relationships laid out above may also be written in terms of velocities related by Jacobians. Flows can be related to piston velocities,

$$\boldsymbol{Q} = -\dot{\boldsymbol{V}} = \mathbf{A}\dot{\boldsymbol{d}}. \quad (10)$$

The jointspace velocities $\boldsymbol{q}$ can be related to the flows $\boldsymbol{Q}$ through the expression

$$\boldsymbol{Q} = \mathbf{A}\mathbf{J_1}(\mathbf{q})\dot{\boldsymbol{q}}, \quad (11)$$

where $\mathbf{J_1}(\mathbf{q}) = \partial \boldsymbol{h}/\partial \boldsymbol{q} \in \Re^{m \times n}$. Thus the matrix $\mathbf{J_1}(\mathbf{q})$ defines the manner in which the cylinders are connected to the joints. The relationship (11) may be expanded to relate taskspace variables $\boldsymbol{R}$ to cylinder flows:

$$\boldsymbol{Q} = \mathbf{A}\mathbf{J_1}(\mathbf{q})\mathbf{J_2^{-1}}(\mathbf{q})\dot{\boldsymbol{R}}, \quad (12)$$

where $\mathbf{J_2}(\mathbf{q}) = \partial \boldsymbol{g}/\partial \boldsymbol{q} \in \Re^{t \times n}$.

In the Cartesian example diagrammed in Fig. 4, it is clear by inspection that $\boldsymbol{R} = \boldsymbol{q}$, and therefore $\mathbf{J_2}(\boldsymbol{q}) = \mathbf{I}$. The pistons of two cylinders are tied together to drive the displacement x while the pistons of another two cylinders are tied together to drive y. Thus the function $\boldsymbol{d} = \boldsymbol{h}(\boldsymbol{q})$ is defined by $d_1 = d_2 = x_0 - x$ and $d_3 = d_4 = y_0 - y$, and the matrix $\mathbf{J_1}(\mathbf{q})$ is constant, taking on the value

$$\mathbf{J_1}(\mathbf{q}) = \begin{bmatrix} -1 & 0 \\ -1 & 0 \\ 0 & -1 \\ 0 & -1 \end{bmatrix}, \quad (13)$$

extensions of the four cylinders. By valve switching ($S_{ij} = \{0, 1\}$), the constraint (7) can impose up to $2^m = 2^4$ valve settings, which in this case correspond to 11 unique directions through the plane (plus free space). The choice of face areas and lever arms will determine the set of directions available in the plane, as we explored previously in [18] with a benchtop transmission setup. This scheme of using valves to multiplex hydraulic lines is called *digital hydraulics* [15]–[17].

There exist several special cases enabled by digital hydraulics which warrant some additional discussion, particularly as they compare to wheeled cobots. The first is the case $\mathbf{S} = \mathbf{0}$. A rolling-contact cobot's natural mode of operation is a constraint; it is the free mode that is difficult to realize. It is only through the use of a feedback loop that the cobot's transmission(s) can be constantly steered in the direction of applied force to accommodate the user's intended instantaneous direction of motion [6]. A digital hydraulic transmission, on the other hand, achieves freespace essentially for free (without feedback control) by opening all cylinders to the reservoir. The ability to render both constraints and free space with our hydraulic transmission also opens the door to more complex virtual environments that feature contact transitions. Unilateral surfaces are easily achieved through a combination of bilateral constraints with free space, and switching between them with load sensing.

In addition to freespace, a digital hydraulic transmission can easily achieve a "motion-locked" mode. By closing all valves (disconnecting the cylinders from both the manifold and the reservoir), each cylinder's motion is blocked[1]. For a rolling-contact CVT to achieve such a behavior, brakes would be required on the wheel axles or force control would be required to constantly steer the wheels so as to oppose the applied force.

C. Modulating The Constraint Using a Hydraulic Transformer

Let us return to the simple two-cylinder example in Fig. 3 and consider an alternative to digital hydraulics. We can instead manipulate the relationship between flows Q_1 and Q_2, in effect modulating the fixed value of −1 that constrains the ratio of flows in (1). Much like electronic transformers that can exchange high voltage/low current for low voltage/high current or mechanical transformers (levers, gears, etc.) that do the same with speed and force, there exist hydraulic transformers that relate flow rate and pressure. One realization is the Innas hydraulic transformer [20].

To maintain generality (and cover the option of tying multiple cylinders in parallel to a given jointspace variable), we shall express the transformer as a relationship among port flows $\boldsymbol{f}$ (invoking the selection matrix $\mathbf{S}$ to relate $\boldsymbol{f}$ and $\boldsymbol{Q}$). And whereas a simple piped manifold imposes only a single constraint, a transformer can impose multiple constraints. That is, the 2-port transformer can be generalized to a multi-port transformer (possibly realized through the connection of several 2-port transformers). In general, a multi-port transformer enforces a matrix relationship $\mathbf{M} \in \Re^{p_{in} \times p_{out}}$ between p_{in} input flows collected in a vector $\boldsymbol{f}_{\boldsymbol{in}} \in \Re^{p_{in}}$

[1]The mathematical formulation described here for $\mathbf{S}$ is limited to valves that always connect the cylinder to either a manifold/transformer port or the reservoir. This "locking" behavior requires different types of valves, which would be a simple extension to this framework

and p_{out} output flows collected in a $\boldsymbol{f_{out}} \in \Re^{p_{out}}$. As given in [21], that relationship may be expressed as

$$\boldsymbol{f_{out}} = \mathbf{M}^T \boldsymbol{f_{in}}. \quad (14)$$

A multi-port transformer imposes as many constraints as the dimension p_{out} of the output vector f_{out}. For a 2-port, this relationship is simply $f_{out}/f_{in} = M$.

We define $\boldsymbol{f} \in \Re^p$, $p = p_{in} + p_{out}$ such that $\boldsymbol{f} = [\boldsymbol{f_{in}}^T, -\boldsymbol{f_{out}}^T]^T$, where all positive flows in $\boldsymbol{f}$ are directed *into* the transformer, to be consistent with (4). We also redefine the matrix $\mathbf{C} \in \Re^{p \times p_{out}}$ such that

$$\mathbf{C}^T = \left[\begin{array}{c:c} \mathbf{M}^T & \mathbf{I} \end{array} \right], \quad (15)$$

with $\mathbf{I}$ a $p_{out} \times p_{out}$ identity matrix. The constraint equation

$$\mathbf{C}^T \boldsymbol{f} = \mathbf{C}^T \mathbf{S} \boldsymbol{Q} = \mathbf{0}, \quad (16)$$

now describes p_{out} scalar constraints, removing as many degrees of freedom from the taskspace motion of the cobot ($DOF = t - p_{out}$).

As a slightly more concrete example, let us return to the example of Fig. 4 and replace the manifold with a 3-port hydraulic transformer. This transformer might take on one of two forms. If the transformer is described as

$$\begin{bmatrix} -f_2 \\ -f_3 \end{bmatrix} = \begin{bmatrix} f_{\text{out},1} \\ f_{\text{out},2} \end{bmatrix} = \begin{bmatrix} M_{1,1} \\ M_{2,1} \end{bmatrix} f_{\text{in},1} = \boldsymbol{M}^T f_1 \quad (17)$$

with 2 outputs and a single input, then two constraints are placed on the flow. In this case, since we only have $t = 2$ to begin with, our hydraulic cobot is locked in place. On the other hand, if our 3-port transformer has 2 inputs and one output such that

$$-f_3 = f_{\text{out},1} = [M_{1,1} M_{2,1}] \begin{bmatrix} f_{\text{in},1} \\ f_{\text{in},2} \end{bmatrix} = \boldsymbol{M}^T \begin{bmatrix} f_1 \\ f_2 \end{bmatrix}, \quad (18)$$

then we are removing a single degree of freedom from the cobot, restricting the end effector to move along a single path.

The two steering methods, digital hydraulics and a variable hydraulic transformer, are illustrated schematically in Fig. 5. Either might be used to realize a hydraulic cobot. It may seem redundant to propose two methods of steering in our framework. However, we do so to explore trade-offs between the two methods. Steering with a continuously variable hydraulic constraint allows us to make direct comparisons between hydraulic and wheeled CVTs. Hydraulic transformer technology is possible (at least in a 2-port realization [20]), but the technology is currently large and heavy, designed to support loads on the order of hundreds or thousands of kg, and is not commercially available yet. On the other hand, controlling the relative flows through a set of valves is physically simple. Cylinders of all sizes are readily available, and the valve bank itself is inexpensive and could feasibly fit in a fanny pack. However, steering methods and behaviors will be quite different from those of wheeled CVTs.

D. Self-Powered Fluid Exoskeletons

While the examples given above introduce how one might realize a fluid cobot, they do not address the aspect that originally motivated a move to fluid transmissions: wearability. For an exoskeleton, the jointspace is parameterized by joint angles which typically align with joints on the body (for example, the shoulder and elbow angles in the plane perpendicular to the axis of the elbow).

Traditional cobot constraints and interaction occur in taskspace through a single interface point, handle, or workpiece. For instance, the rehabilitation cobot in [7] defines paths along which the user's hand should move. An exoskeleton, on the other hand, interacts with the user primarily in jointspace. A constraint defined in jointspace might also be viewed as akin to an enforced motion synergy, which may be of interest for patients recovering from a stroke or head injury [22]. The hydraulic constraint-imposing exoskeletons we propose here are effectively a new class of cobot — one that differs in both the transmission type and the mode of interaction with the user. The difference is more a conceptual one than a mathematical one, since hydraulics could easily be used to achieve endpoint-interaction cobots, and many exoskeleton constraints could be defined in taskspace. For simplicity, we will still discuss all constraints as existing in taskspace, with the caveat that by definition $\mathbf{J_2} = \mathbf{I}$ if the constraint is a joint coordination.

To clarify these differences, we will discuss two hydraulic exoskeleton examples: design A is an n-joint exoskeleton that forms a kinematic chain to be worn on one limb, and design B is an n-joint exoskeleton with $n/2$ joints to be worn on each of two homologous limbs. In either case, we assume that each joint is spanned by cylinder(s) connected by digital hydraulics and/or a variable hydraulic transformer. Upper-body $n = 2$ examples of these two designs are shown in Fig. 6.

Typically, a virtual wall is rendered in taskspace to augment the physical environment in which manipulation occurs. This functionality can be achieved by design A, which spans the user's arm, and can impose constraints in taskspace defined by the hand position.

Paths defined for design B instead correspond to joint coordinations; applications in which homologous limbs work together are quite common (for example, walking or reaching for an

object with two arms). Mathematically, we still use taskspace ($\mathbf{J_2} = \mathbf{I}$, as discussed previously) to describe these paths, with the understanding that it has no physical meaning.

E. Parasitic Effects

While ideal transmissions can achieve perfect performance, physical realizations are plagued by parasitic effects. Regardless of whether a constraint is realized with hydraulic or rolling transmissions, a user will naturally feel the reflected inertia of the device and the friction in its joints. With rolling contacts, the user will additionally feel the friction in the roller bearings of the wheel (assuming the controller steering the wheel can keep up with the applied forces when free space is rendered), which will be quite small. In place of this bearing friction, hydraulics will naturally generate frictional forces in cylinder piston and rod seals as well as fluid losses. Such losses can be minimized by design. For example, the authors of [23] have developed a very low-friction hydraulic transmission using rolling diaphragm cylinders.

The rendered constraints will also display certain nonlinearities under large loads. In rolling transmissions, these parasitics take the form of sideslip: the adherence of a wheel to its desired direction of motion is limited by the relationship between the force $F_\perp$ perpendicular to its direction of motion and the force F_N normal to the surface it rolls on [24] (Fig. 7a). At a certain point, $F_\perp$ overcomes the wheel's sticking friction limit and the wheel slips sideways. To avoid such slip, some cobot designs have resorted to CVTs that support high normal forces (for example, [14] uses wheels with about F_N = 250N preload).

Whereas a rolling constraint will slip if contact forces are not sufficiently high to resist perpendicular forces, a hydraulic transmission does not easily "slip," since flow across the piston is easy to prevent. Hydraulic transmissions are widely used in large-load applications without exhibiting leakage across seals. In fact, given a truly incompressible hydraulic fluid, any loads up to the pressure limitations of the cylinders, valves, and tubing in the hydraulic circuit can be supported without slip.

In reality however, no fluid is completely incompressible, particularly if it is acting at low pressure. Instead, fluids are characterized by a bulk modulus, such that the elasticity of the fluid is determined by the fluid itself, the operating pressure, and the total volume. Instead of slipping off the desired path when large normal forces are applied by the user, the fluid cobot displays a "stretch" of the nominal path due to fluid compliance, and springs back to the desired path when the normal force is removed (Fig. 7b). Even without "steering corrections" realized through feedback control, a hydraulic constraint's anchor position can be maintained at its original coordinates, with increased force resulting as penetration increases into the constraint.

III. Fluid Cobot Kinematics

The programmable relationships that can be modulated through the matrices **C** and **S** constrain the cylinder flows $\boldsymbol{Q}$ to lie within certain mathematical manifolds or paths. However, paths of interest are unlikely to be defined in terms of fluid flow relationships; rather, they would be defined in taskspace as limb endpoint motions or joint relationships.

At this "highest" taskspace level, a cobot as originally proposed has a single unconstrained degree of freedom, with all other directions of motion constrained by the transmissions [6] (although higher DOF "minimally constrained" cobots have been proposed [25]). Due to the CVTs, the constrained direction cannot be altered instantaneously; rather, the cobot must always steer along a curve. Since the velocity is controlled by the operator, a controller can only impose the turning rate or derivative of the transmission ratio.

To steer motion, cobots traditionally use controllers based on the geometry of curves [19]. When a path is parametrized by its length s, the direction and speed along a path can be separated. The operator's input is described as the motion along the path ($s, \dot{s}. \ddot{s}$). The resulting taskspace velocity $\dot{\boldsymbol{R}}$ depends on the constrained heading

$$\boldsymbol{T} = d\boldsymbol{R}/ds, \quad (19)$$

with $d\boldsymbol{R}/dt = \boldsymbol{T}\dot{s}$. Furthermore, a similar relationship holds for the second derivative,

$$d\boldsymbol{T}/ds = \kappa \boldsymbol{N}, \boldsymbol{N} \perp \boldsymbol{T}. \quad (20)$$

By controlling the curvature κ, the controller influences $\boldsymbol{T}$ to select a path independently of the operator-defined path speed.

Thus, we expect a controller for a cobot with a CVT (rolling contact or hydraulic) to set a path curvature based on the current configuration and desired position in taskspace. Or, in the case of digital hydraulics, to select from a set of available directions the one which points towards the desired path. These quantities live in taskspace and must be related to the flow constraint we can directly manipulate. There are two options for addressing this challenge, illustrated in Fig. 8. The method of Fig. 8a requires transforming complete paths, which may not always be feasible. The method of Fig. 8b only requires transforming points, headings, and curvatures, all of which have been previously derived for traditional cobots [19]. The additional spaces defined here are motivated by the desire to define programmable constraints in taskspace, and then to implement them by manipulating C or S as in Fig. 8b.

A. Coupling Space

The first space we define will be motivated by the hydraulic implementation of the variable constraint. The flows $\mathbf{Q}$ constrained by (16) are the derivatives of volumes $V_1, \ldots, V_m$ inside the cylinders. Since $\mathbf{C}^T\mathbf{S}$ (the setting over which we have control) relates the volumes, it is necessary to convert the desired motion towards the path in taskspace into the space of these volumes, as in Fig. 8b. Thus, we will define a set of *coupling spaces* spanned by these volumes, with a coupling space for each constraint present.

Since the constraint equation (16) contains p_{out} scalar equations, we have a set of p_{out} coupling spaces. Each of these scalar equations defines an output flow in terms of its relationship to all of the input flows. Thus, we define our coupling spaces as $\Sigma_1, \ldots, \Sigma_{p_{out}}$, where each space Σ_i is spanned by the axes $V_1, \ldots, V_m$. We will examine separately the

simplifications available to these coupling spaces when steering with either transformer ratios (with **C**) or by switching a digital hydraulic transmission (with **S**).

1) Steering with a hydraulic transformer—Let us begin with steering by manipulation of the matrix **C** during which times we assume that **S** is fixed. Ultimately, we would like our controller to calculate a derivative of **C**, such that we might continuously vary our transmission ratios. However, our coupling space definition limits us to looking at the lumped matrix $\mathbf{C}^T\mathbf{S}$. The fixed matrix **S**, however, will likely have a very simple structure (for example, the identity matrix), since cylinder redundancies have no great value when a hydraulic transformer is present, and cylinders on a single joint could be reduced to a single effective cylinder area. Thus, we can reduce the number of axes in each coupling space, eliminating those with entries of 0 in **S**.

In the case **S** = **I**, where a single cylinder is connected to each transformer port ($p = m$), the axes of the ith coupling space Σ_i will thus reduce (due to the form of the matrix **C**) to the $p_{in} + 1$ dimensional set of axes $V_1, \ldots, V_{p_{in}}$ and $V_{p_{in}+i}$, such that each coupling space contains the volumes of all the cylinders connected to the input ports and a cylinder connected to a single output port[2]. Even when $S \neq I$, there exists a simple, non-state dependent relationship between $\boldsymbol{V}$ and the volumes connected to each transformer port.

2) Steering with digital hydraulics—On the other hand, when we steer with a digital hydraulic transmission by changing **S**, we can make the assumption that no hydraulic transformer is used, and only a simple manifold is present ($\boldsymbol{C}^T = [1, \cdots, 1]$). Any valve setting that is selected corresponds to an allowed direction of motion in the single coupling space Σ with axes spanned by the cylinder volumes.

The single hydraulic manifold in the digital hydraulic transmission described above ($p_{out} = 1$) restricts only a single degree of freedom. Thus, if restriction of motions to a single path is desired for cobots of higher dimensionality, it is necessary to introduce multiple independent manifolds. This is possible in our mathematical framework; for example, two independent hydraulic manifolds might be described by

$$\mathbf{C}^T = \begin{bmatrix} 1 & \cdots & 1 & 0 & \cdots & 0 & 1 & 0 \\ 0 & \cdots & 0 & 1 & \cdots & 1 & 0 & 1 \end{bmatrix}. \quad (21)$$

In this case, there would be two m-dimensional coupling spaces[3] Σ_1 and Σ_2.

3) Comparison with rolling-contact CVT coupling spaces—These coupling spaces are similar to those defined for rolling contacts. In both cases, each coupling space is spanned by axes of the variables whose derivatives are related by the constraint. For either hydraulic steering method, the volumes are analogous to the x_i and y_i directions that form the coupling space Σ_i for a rolling constraint in a wheeled cobot.

[2]If **M** contains some elements that are always 0, further reduction may be possible, but this is the general form.
[3]If we know that by design, certain cylinders can only be connected to a single manifold, placing restrictions on **S**, we can further reduce the dimensionality of each coupling space.

It should be noted that previous cobot realizations all had 2-dimensional coupling spaces due to the use of wheeled contacts, whereas fluid coupling spaces can be of higher dimension. It may seem restrictive to consider two-dimensional coupling spaces at all for hydraulic cobots, but the requirements which result in 2D coupling spaces are fairly straightforward — in fact, all we need require is that we remove redundancy in joints ($n = t$) and cylinders, and that we design to allow only a single degree of freedom.

If a transformer is used for steering, letting $\mathbf{S} = \mathbf{I}$ by design is quite logical (as noted previously) — this implies $p = m$. The only additional assumption we need make is that we have the same number of cylinders as joints ($n = m$). Provided the cobot is designed with a single degree of freedom, we must have $p_{out} = t - 1$ constraint equations, so $p_{in} = p - p_{out} = 1$. This leaves us with p_{out} 2-dimensional coupling spaces, where the ith space is spanned by the volumes V_1 and V_{i+1}.

B. Steering Space

Given a framework for describing coupling spaces where constraints impose direct non-state-dependent relationships, we now address how we might control such constraints. For a hydraulic cobot, we have defined p_{out} coupling spaces $\Sigma_1, \cdots, \Sigma_{p_{out}}$, each spanned by a set of cylinder volumes. We have already alluded to the fact that constraints correspond to allowed directions of motion in these coupling spaces. We will define the *steering space(s)*, one per coupling space, with variables parameterizing these allowed directions of motion. It is these variables, then, that must be manipulated to steer the cobot, setting the stage for closed-loop steering control.

In general for hydraulic cobots, flows $\mathbf{Q}$ are allowed in any direction in the nullspace of the constraint; that is, flows are allowed perpendicular to the matrix $\mathbf{S}^T\mathbf{C}$. In each of the p_{out} coupling spaces, then, flow is restricted to a p_{in} dimensional mathematical manifold satisfying (16). As with the couping spaces, we will examine the steering space in terms of the simplifications possible when certain assumptions are made about $\mathbf{S}$ or $\mathbf{C}$.

1) With a hydraulic transformer—Let us begin with the case where $\mathbf{S} = \mathbf{I}$ and all steering is done through manipulation of $\mathbf{C}$. Furthermore, let us assume that the conditions enumerated in the last paragraph of the previous section are met: $t = n = m = p$ and $p_{out} = t - 1$, such that we have p_{out} 2-dimensional coupling spaces Σ_i. For each of these coupling spaces, the instantaneous allowed direction of motion corresponds to a heading ϕ_i in Σ_i that is precisely analogous to the steering angle for a wheeled cobot. We recall that for a hydraulic transformer with $p_{in} = 1$, our constraint can also be written in the form

$$\boldsymbol{f}_{\boldsymbol{out}} = \mathbf{M}^T f_{in} = [M_1 \cdots M_{p_{out}}]^T f_{in}. \quad (22)$$

Since $\boldsymbol{f} = \boldsymbol{Q}$, the headings can be related to the transformer by the relationship

$$tan(\phi_i) = M_i. \quad (23)$$

Collection of these variables into a $p_{out} = n - 1$ dimensional vector gives us the *steering space*,

$$\mathbf{\Phi} = [\phi_1 \cdots \phi_{p_{out}}]^T, \quad (24)$$

which describes the instantaneously allowed direction of flow, and can be used to compute $\boldsymbol{M}$ as in (23).

What happens when we relax the assumptions above? Namely, what is the result when we no longer require that $p_{out} = n-1$? Flow is then restricted to a constraint *manifold* rather than a path, and coupling spaces are no longer necessarily 2-dimensional. Without limiting the cobot's motion to a 1-DOF manifold by design, we are no longer able to constrain paths at all. Methods like those used by Hodgson et al. in [25] can be used to converge to a manifold; however, the controller developed by Hodgson et al. still depends on steering in 2-dimensional coupling spaces.

2) With digital hydraulics—On the other hand, for a cobot that tracks a desired path using a switched digital hydraulic transmission, we can simplify the constraint (16) as follows:

$$0 = \boldsymbol{C}^T \mathbf{S} \boldsymbol{Q} = [1, \cdots, 1] \begin{bmatrix} s_{11} & \cdots & s_{1m} \\ \vdots & \ddots & \vdots \\ s_{p1} & \cdots & s_{pm} \end{bmatrix} \boldsymbol{Q} = \left[\sum_{i=1}^{p} s_{i1}, \sum_{i=1}^{p} s_{i2}, \cdots, \sum_{i=1}^{p} s_{im} \right] \boldsymbol{Q} \quad (25)$$

$$= [\tilde{s}_1, \tilde{s}_2, \cdots, \tilde{s}_m] \boldsymbol{Q} = \tilde{\boldsymbol{S}}^T \boldsymbol{Q}.$$

Since S can contain at most a single nonzero entry in each column, each element $\tilde{s}_j = \sum_{i=1}^{p} s_{ij}$ (with $j \in 0, 1, \cdots, m$) must be either a 0 or a 1. This simplification makes it clear that there are, at most, 2^m possible transmission ratios, each corresponding to a hyperplane (tangent space) in the coupling space, some of which can be co-planar. Thus, fluid is restricted to flow only in directions in the set

$$\tilde{\boldsymbol{S}}^{\perp} = span\{\boldsymbol{Q} \in \Re^m | \boldsymbol{Q} \perp \tilde{\boldsymbol{S}}\}. \quad (26)$$

The steering space may thus be parametrized by any set of vectors spanning $\tilde{\boldsymbol{S}}^{\perp}$. For multiple independent hydraulic manifolds, each manifold can then be analyzed independently as described above for its allowed directions of motion based on the subset of $\boldsymbol{S}$ that is selected by each row of C.

Of course, this set of directions could also be expressed as headings, but there is no motivation for development of a continuous steering space in a digital hydraulic

transmission. Enumeration of $\tilde{\boldsymbol{S}}^{\perp}$ for each available valve setting provides information about all possible steering directions. Since the configuration in coupling space is selected from a discrete available set rather than a continuous one, a hybrid control scheme is required to select valve settings from this finite set rather than calculate a derivative for steering. It is desirable to enumerate these directions in a non-state-dependent space (as a set of possible configurations, $\tilde{\mathbf{S}}^{\perp}$) rather than to re-calculate them continuously in taskspace.

C. Transformations Between Spaces

Recall that we previously defined a relationship (9) which allows us to solve for the configuration in coupling space from the taskspace configuration (as long as we avoid singularities and mechanical redundancies).

Since our controller needs to manipulate the direction of motion, we convert between spaces not only the configurations, but also path headings and curvatures. These transformations, derived in [19], are recapped briefly here. In general, converting headings through different spaces is achieved through the use of Jacobian matrices dictated by the cobot's geometry. For configurations $\boldsymbol{a}$ and $\boldsymbol{b}$ in any two spaces related by an equation $\boldsymbol{a} = \boldsymbol{\psi}(\boldsymbol{b})$, the unit tangent vector (heading) $\boldsymbol{T}_b$ in space B can be converted to $\boldsymbol{T}_a$ in space A through a relationship imposed by the Jacobian $\mathbf{J} = \partial\boldsymbol{\psi}/\partial\boldsymbol{b}$:

$$\boldsymbol{T}_a = \frac{\mathbf{J}\boldsymbol{T}_b}{|\mathbf{J}\boldsymbol{T}_b|}, \quad (27)$$

In order to transform not only the current heading, but also a desired steering command between spaces, an additional transformation of curvature is required. Curvature is defined with the vector $\boldsymbol{\kappa}_b\boldsymbol{N}_b$ in space B (where $\boldsymbol{N}_b \perp \boldsymbol{T}_b$), and can be transformed into space A using the equation

$$\kappa_a \boldsymbol{N}_a = \frac{[\mathbf{I} - \boldsymbol{T}_a\boldsymbol{T}_a^T]}{|\mathbf{J}\boldsymbol{T}_b|^2}[\boldsymbol{T}_b^T\frac{\partial\mathbf{J}}{\partial\boldsymbol{b}}\boldsymbol{T}_b + \mathbf{J}\kappa_b\boldsymbol{N}_b], \quad (28)$$

where the shorthand term $\boldsymbol{T}_b^T\frac{\partial\mathbf{J}}{\partial\boldsymbol{b}}\boldsymbol{T}_b$ indicates

$$\left\{\boldsymbol{T}_b^T\frac{\partial\mathbf{J}}{\partial\boldsymbol{b}}\boldsymbol{T}_b\right\}_i = \sum_{j=1}^{n}\left[\sum_{k=1}^{n}\frac{\partial J_{(ij)}}{\partial\boldsymbol{b}_{(k)}}\boldsymbol{T}_{b(k)}\right]\boldsymbol{T}_{b(j)}. \quad (29)$$

We now prepare to address the control of a variable transmission that relates the taskspace variables x and y by a desired path. As discussed previously, we have two methods of steering: through a continuously variable transformer or a switched digital hydraulic system. In this work, we will consider in detail only a steered transmission realized through a variable hydraulic transformer that steers through the matrix $\mathbf{C}$. We build on the control

scheme for CVTs laid out in [19] for rolling-contact cobots. In the following section, we present a similar, but slightly simpler, controller for computing a steering angle $\dot{\Phi}$. We leave the development of a hybrid control scheme to realize switching between sets of dynamics with digital hydraulics for future work.

IV. Steering Controller for a 2-D Hydraulic Transformer

Our controller for following a path using a hydraulic transformer takes the form of a "lookahead" controller, as presented in [26], with additional inspiration taken from [19]. The lookahead controller operates in taskspace, as illustrated in Fig. 9a.

Coulter's algorithm [26] works to select a curvature as illustrated in Fig. 9b: a goal point R_p on the desired path is selected by computing the closest point on the desired path, and then searching forward along the path until the distance between the current configuration $\boldsymbol{R}$ and that point is equal to the lookahead distance ℓ. The controller computes the error

$$\boldsymbol{e}_{\boldsymbol{global}} = \boldsymbol{R}_{\boldsymbol{p}} - \boldsymbol{R} \quad (30)$$

in taskspace where the path is defined. Transformation of error to the local frame is done by aligning the local y-axis with the path tangent vector T_R in taskspace and performing a simple rotation on the vector $\boldsymbol{e}_{\boldsymbol{global}}$ to produce $e_{local} = [e_x, e_y]^T$. Then, the desired curvature in taskspace is calculated using the x-component of that local error,

$$\kappa_R = -2e_x/\ell^2. \quad (31)$$

To adapt Coulter's controller to cobots, we then transform the curvature to coupling space using equations (27–29). The curvature in coupling space and the path velocity v are used to compute the coupling space angular steering rate, $\dot{\phi} = \kappa_v(\lambda_v)$, the integral of which is enforced by selecting the transmission ratio M for the transformer. The lookahead controller is tuned by determining the lookahead distance ℓ; the choice of ℓ determines how sharply the commanded path converges towards the desired one. An additional tuning gain λ that was not used in [26] or [19] is introduced to the calculation of the steering rate $\dot{\phi}$; it simply amplifies the path velocity as though it were computed in different units, which speeds up the steering. It should be noted that this control scheme, like the one in [19], is applicable only to cobots which have 2-dimensional coupling spaces.

Since there is no explicit check for the stroke limits in the control scheme, it is important that the desired path be designed to fall within the reachable envelope. Additionally, the path from $\boldsymbol{R}$ to $\boldsymbol{R}_{\boldsymbol{p}}$ may fall outside this envelope, particularly when the envelope is non-convex or when the user is near (and moving towards) the edge of the envelope. Use of a sufficiently small ℓ can mitigate these effects.

V. Experimental Evaluation

To support the theoretical development, we have prototyped a simple 2-joint hybrid digital/continuous hydraulic exoskeleton, with which we examine free space and constraint rendering. It features a set of valves which can connect the two cylinders either to a common manifold or to the reservoir:

$$\mathbf{S} = \begin{bmatrix} S_{11} & 0 \\ 0 & S_{22} \end{bmatrix}, \quad (32)$$

as well as a hydraulic transformer imposed between the two cylinder flows:

$$\mathbf{C}^T = [M\ 1]. \quad (33)$$

By introducing variability in both **S** and **C**, the prototype has the ability to achieve constraints and free space in two ways:

1. using **S**, free space can be achieved at little cost by opening both cylinders to the reservoir, and a fixed constraint can be rendered based on the relative face areas of the cylinders, or
2. using **C**, programmable constraints can be achieved by changing the transmission ratio *M*, or free space can be rendered as in traditional cobots — by measuring forces and steering in the direction of applied force.

One could also use this setup to achieve a “best of both worlds” scenario, in which steering is achieved through the hydraulic transformer and free space is rendered by simply using switches to connect the cylinders to the reservoir. However, for the sake of clarity, we will examine these two methods separately.

In addition to the two methods of “steering,” the device can be configured to realize two exoskeletons, one of each configuration described previously: either a kinematic chain spanning the shoulder and elbow, or a link between the two elbow joints on opposite arms, as in our design A and B examples of Fig. 6.

A. Exoskeleton Apparatus

The prototype exoskeleton connects either the shoulder and the elbow or opposite elbows through identical cylinders (Bimba SR-046-DPY-00MC) spanning each of the two joints. The device is mounted to a table above the stationary shoulder or elbow joint, and is supported by ball transfers (McMaster 6460K31) under the moving arm segments. The joints are instrumented with rotary incremental encoders (US Digital E2-2048-375-IE-D-D-B). Water is used as the hydraulic fluid, and the reservoir is maintained at atmospheric pressure. The operator’s arm rests in two cuffs, and interaction forces with the robot are measured using beam load cells (Transducer Techniques LSP-5) mounted between the cuffs and the exoskeleton. The shoulder-elbow setup of the prototype as used for switching with **S**

is shown in Fig. 10, and the elbow-elbow setup simply duplicates the pictured elbow joint on the opposite arm (without making use of the shoulder joint).

B. Exoskeleton Kinematics

The two cylinders and two valves on the exoskeleton prototype yield a 2-dimensional coupling space parametrized by (V_1, V_2). The mounting of a single cylinder across each joint q yields a diagonal Jacobian matrix, imposing the ideal (incompressible fluid) relationship $\boldsymbol{d} = h(\boldsymbol{q})$ determined by the geometry. For the shoulder-elbow configuration shown in Fig. 11, the relationship can be expressed as

$$\begin{bmatrix} d_1 \\ d_2 \end{bmatrix} = \begin{bmatrix} z_0 - \sqrt{z_1 - z_2 \cos(q_1 - z_3)} \\ z_4 - \sqrt{z_5 - z_6 \cos(z_7 - q_2)} \end{bmatrix}, \quad (34)$$

where constants $z_0, \cdots, z_7$ are determined by the mounting geometry (and are different for the elbow/shoulder and elbow/ elbow configurations). For the elbow-elbow configuration the relationship is instead

$$\begin{bmatrix} d_1 \\ d_2 \end{bmatrix} = \begin{bmatrix} z_0 - \sqrt{z_1 - z_2 \cos(z_3 - q_1)} \\ z_4 - \sqrt{z_5 - z_6 \cos(z_7 - q_2)} \end{bmatrix}. \quad (35)$$

Taking the derivative yields an expression of the form

$$\dot{\boldsymbol{d}} = \mathbf{J_1}(\mathbf{q})\dot{\boldsymbol{q}} = \begin{bmatrix} J_{1,1}(q) & 0 \\ 0 & J_{1,2}(q) \end{bmatrix} \dot{\boldsymbol{q}}, \quad (36)$$

where $J_{1,i} = \frac{\partial h_i}{\partial q_i}$ is defined by the geometric relationship $d_i = h_i(q_i)$ imposed by the mounting of the cylinders.

Fixing $\boldsymbol{C}^T = [1, 1]$, the constraint in (25) imposes $\boldsymbol{C}^T\mathbf{S} = [\tilde{s}_1, \tilde{s}_2]$, where $\tilde{s}_1$ and $\tilde{s}_2$ can each take on values of either 0 or 1. The constraint can be written as

$$\tilde{s}_1 Q_1 + \tilde{s}_2 Q_2 = \tilde{s}_1 A_1 \dot{d}_1 + \tilde{s}_2 A_2 \dot{d}_2 = \tilde{s}_1 A_1 J_{1,1}(q)\dot{q}_1 + \tilde{s}_2 A_2 J_{1,2}(q)\dot{q}_2 = 0\,. \quad (37)$$

Thus, when both cylinders are connected to the manifold ($\tilde{s}_1 = \tilde{s}_2 = 1$), the constraint $\dot{d}_1/\dot{d}_2 = -A_2/A_1$ is imposed, which creates the nonlinear jointspace relationship

$$\frac{\dot{q}_2}{\dot{q}_1} = -\frac{A_1 J_{1,1}(q)}{A_2 J_{1,2}(q)}\,. \quad (38)$$

For the elbow-shoulder configuration (design A), a further transformation can be made to describe the constraint in taskspace. The kinematic chain enforces the nonlinear relationship $\boldsymbol{R} = \boldsymbol{g}(\boldsymbol{q})$, where $\boldsymbol{R}$ is the (x, y) position of the hand in the plane.

$$\boldsymbol{R} = \begin{bmatrix} x \\ y \end{bmatrix} = \begin{bmatrix} -z_8 \cos(q_1) - z_9 \cos(q_1 + q_2) \\ z_{10} \sin(q_1) + z_{11} \sin(q_1 + q_2) \end{bmatrix}, \quad (39)$$

where $z_8, \cdots, z_{11}$ are constant link lengths. Since both taskspace variables depend on both joint angles, $\mathbf{J_2}(\boldsymbol{q})$ cannot be simplified by placing zeros on the off-diagonal.

For the elbow-elbow configuration (design B), we instead simply have $\boldsymbol{q} = \boldsymbol{R}$ and $\mathbf{J_2}(\boldsymbol{q}) = \mathbf{I}$.

C. Switching Apparatus

A set of 3-port diverting valves (McMaster 46095K21) allows the two cylinders to be connected to each other ($\mathbf{S} = \mathbf{I}$ imposes $M = -1$) or to the reservoir.

D. Hydraulic Transformer Apparatus and Control

As discussed previously, hydraulic transformers do exist in physical realizations [20], but they are not intended for use at the scale of human interaction. Rather than realizing a true hydraulic transformer, we introduce an electromechanical teleoperator between the two cylinders of the desktop exoskeleton prototype to serve as a “virtually variable hydraulic transformer” (VVHT). The purpose of the teleoperator is twofold: 1) It imposes (in software) the constraint that a hydraulic transformer would achieve, and 2) it enables compensation for parasitic loads arising from seal friction in off-the-shelf hydraulic cylinders. Still, the use of a teleoperator ensures that, despite the use of an active device, no power is inserted into the system beyond what is required to match power between the input and output joints. The addition of the electromechanical link reintroduces the motors that the hydraulic transmission sought to eliminate, but preserving the cylinders as a point of interaction with the operator allows the heavy components to be placed remotely, while the exoskeleton-mounted cylinders are simply tethered by flexible tubing. In order to distinguish from the “outer loop” steering controller discussed in Section IV, we will refer to the control scheme that imposes the transformer constraint as the “inner loop”.

1) VVHT apparatus—The hydraulic inputs to the VVHT are routed to a second set of cylinders (Bimba HLM-067-DT1) which are mechanically coupled to the motion of two permanent magnet DC motors (Bodine Electric 6022) through custom capstan drives and linear slides (Misumi SV2R24-340), as shown in Fig. 12. Thus, instead of being connected by direct fluid flow, the exoskeleton’s cylinders are virtually connected by the teleoperator. The motor angular displacements are instrumented with digital rotary encoders (US Digital E3-2500-500-IE-H-D-B) mounted to the output shaft. While position and velocity data are still collected at the exoskeleton cylinders, the encoders colocated with the motors are used to close the control loops since they are higher resolution. The capstan drive produces 30.1 mm of piston travel for each revolution of the motor shaft. Data collection/logging and

control was performed in Microsoft Visual Studio/C++ code with a Sensoray Model 626 card for data acquisition.

2) Inner Loop Transmission Ratio and Free Space Enforcement—In order to use the VVHT as a stand-in for a hydraulic transformer, we restrict the controller to act like its desired physical equivalent. Despite the fact that a separate motor controls each joint on the exoskeleton, we do not compute motor command signals as though we were performing position control of a standard 2-link holonomic manipulator. Instead, to realize a variable transformer, we constrain the 2 DOF system through a teleoperator transmission ratio to a single DOF. This is achieved through the realization of a scaled teleoperator between the two motors, which attempts to preserve power by scaling both flow and pressure (velocity and force).

Past work on teleoperators with non-unity transmission ratios or scaling focused primarily on a local and remote device that operated in vastly different scales (micro-manipulation or manipulation of large loads by a human), choosing fixed scaling ratios (optionally with different ratios for force and position scaling) appropriate to the operator and remote workspaces [27], [28]. If, however, the teleoperator's transmission ratio is allowed to vary during operation, and if the forces are scaled inversely to the velocities, the teleoperator effectively functions as a variable ratio transformer.

We close two inner proportional control loops, realizing a 2-channel force-position teleoperator. In the implemented configuration, the master joint (shoulder) of the exoskeleton operates as an admittance device and the slave joint (elbow) operates as an impedance device [29] as shown in Fig. 13. The desired forces and velocities (flows and pressures) for the two inner loops are related to the user- and environment-generated values by the transmission ratio. In order to prevent instability resulting from large amplification of motions or forces by M, transmission ratio magnitudes were limited to the range of [0.25, 4], although the heading angle ϕ continued to update in the outer loop controller discussed in Section IV[4].

To realize freespace, an admittance controller is imposed. Proportional control regulates the interaction forces applied by the operator, attempting to drive them to zero. This is similar to steering a wheeled cobot in the direction of applied force.

E. Methods

1) Experiment 1 — Free Space and Constraints with Switching—We performed a simple experiment to compare our digital hydraulic transmissions with rolling contacts. In [6], results are given for steering the Unicycle cobot through freespace until it hits a wall, traveling along that wall while supporting load, and then leaving the wall. We reproduced this behavior with both configurations A and B of the digital hydraulic cobot, fixing $M = 1$ (bypassing the VVHT).

[4]Introduction of a variable transmission ratio to a scaled teleoperator poses unique stability challenges. With simple fixed-gain proportional controllers in the force and position loops of a 2-channel teleoperator, large transmission ratios pose challenges. Exploration of the stability to achieve transmission ratios outside this constrained range was considered outside the scope of this work, but is an interesting problem that warrants further exploration.

2) Experiment 2 — Free Space and Constraints with the VVHT—To compare the steered and digital transmission renderings of both free space and the virtual constraints, data were collected for motions using the VVHT that start in free space, hit a guiding surface constraint, and then leave the constraint, just as was done in Experiment 1. Of course, the digital transmission highlighted above in Experiment 1 could only draw a straight line through coupling space with a slope of −1; transformed through the Jacobian and cylinder face area ratios, this became a curve in jointspace. The VVHT, however, is programmable; to demonstrate this, the constraint in question was programmed to be a straight line through jointspace, which requires modifying the transmission ratio M between the motors on-the-fly. The valves are set to $\mathbf{S} = \mathbf{I}$.

3) Experiment 3 — Complex Constraint with the VVHT—Of course, the programmability of the virtual transmission gives it flexibility to do much more than render straight-line constraints. As a more illustrative example of the variable transmission, a path consisting of two line segments was also imposed. The selected path might be useful for a stroke patient to exercise their full range of motion at the elbow by forcing them to move it twice through this range for each motion they make with their shoulder. The valves are set to $\mathbf{S} = \mathbf{I}$.

VI. Results and Discussion

A. Experiment 1 — Free Space and Constraints with Switching

Sample trajectories and measured forces for the wheeled and digital hydraulic transmissions are given in Fig. 14 and Fig. 15. A comparison of these simple examples illustrates some of the important differences between a constraint realized with rolling contact transmissions and one realized with digital hydraulic transmissions. As the Unicycle cobot reaches the virtual surface, it actually penetrates the wall, then steers back out. Since the cobot is displaying free space before it hits the constraint, the wheel is pointed into the wall, and it must then use feedback control to steer back out even while the user continues pushing farther into the virtual wall. In contrast, a digital hydraulic transmission can instantaneously switch from free space to a constraint with the flip of a valve, without making use of feedback.

In [6], Peshkin et al. discuss the challenge of attempting to make the Unicycle cobot isotropic (able to respond equally well in free-space to forces parallel to and perpendicular to the current direction of motion). Whenever the path velocity is nonzero, the path cannot instantaneously change direction. However, the authors found that at low speeds (a few cm/s), the behavior felt “qualitatively isotropic.” The advantage of the digital hydraulic free-space realization is that no transmission ratio need be imposed or actively controlled when all cylinders are simply opened to the manifold. Rather than generating high operator forces when trying to turn sharply, the forces in free space tend to stay at a relatively constant magnitude, as shown in Fig. 16, and the constraint realized using the hydraulic cobot is very isotropic.

As can be seen in Fig. 15, the compliance of the hydraulic transmission allows some penetration into the constraint under load, causing the constrained path to differ from the

predicted constraint. This could be minimized through the use of a pressurized working fluid. Additionally, the relatively high free-space loads that characterize this digital hydraulic transmission could be reduced if rolling diaphragm cylinders were employed instead of cylinders with piston seals [23]. This would make the contrast between constraints and free space motion even more stark.

B. Experiment 2 — Free Space and Constraints with the VVHT

Fig. 17 shows results for a straight line drawn through jointspace. The transmission ratio computed by the outer loop to impose the constraint is shown in the middle pane of the figure, along with the measured forces during free space in the bottom pane.

For the teleoperated VVHT apparatus, the performance of the inner teleoperator control loops was limited by noisy force signals, as well as a significant dead-band in the motor response near zero command input. These inner loop limitations influenced the performance of the outer steering control loop, since they resulted in the realization of a non-ideal transmission ratio. However, despite these limitations, the position tracking ability even in the open loop was comparable to the direct hydraulic transmission, but resulted in significantly lower forces between the operator and the exoskeleton, as shown in the comparison between torques reported in Fig. 16 and Fig. 17. Thus, in addition to adding transmission ratio flexibility, the VVHT was able to compensate for much of the friction and stiction present in the hydraulic and mechanical components of the tabletop exoskeleton.

C. Experiment 3 — Complex Constraint with the VVHT

The flexible transmission ratio allowed for steering along a path that is clearly not achievable with a fixed transmission ratio, as shown in Fig. 18. The position reading colocated with the motors (green line in the top pane of Fig. 18) clearly tracked the desired constraint well, while the compliance in the hydraulic fluid led to significant joint angle differences measured at the exoskeleton joints themselves (gold line).

Ideally, the force and position measurements for the VVHT's teleoperator scheme would be colocated at the exoskeleton joints. As mentioned in Section V, our position loop is instead closed between the two motor shafts in our implementation since the motor encoder resolution is approximately 25 times higher due to capstan gearing. The assumption made in this implementation is that the dynamics between the motor and the exoskeleton cylinder are negligible. However, as discussed previously (see Fig. 7), we have compliance in our hydraulic lines due to the low operating pressure. These dynamics are actually somewhat realistic when looking forward to our digital hydraulic implementation, since line length and fluid compressibility may still present challenges.

VII. Conclusion

In this paper, we have introduced the mathematical framework to support a new wearable rehabilitation robot technology based on hydraulic transmissions. Inspired by cobots, these body-powered exoskeletons have the potential to achieve freespace and slip-free constraint surfaces, potentially without the need for force measurement.

Both the physical and virtual transmissions successfully rendered virtual constraints and free space. Free space forces were lower with the virtual transmission (due to compensation), but free space was much easier to achieve with digital hydraulics (simply open the cylinders to the reservoir). Both transmissions supported loads against their guiding surfaces without slipping, though the rendered guiding surfaces showed a certain amount of compliance. The physically-constrained path exhibited smaller excursions from the desired path than the VVHT-constrained one under similar loads; both the compliance of the control gain and the additional compliance of longer hydraulic lines connecting the wearable portion of the cobot to the VVHT contribute to this difference. In looking at these results, we must keep in mind that our VVHT is not truly a variable hydraulic transformer.

Our future plans include physical realization and control of a more complex digital hydraulic exoskeleton, since the VVHT was a research tool, not a final realization. One of the challenges of working with a digital hydraulic transmission is that the available transmission ratios are determined by the mechanical design, so they are relatively difficult to change. The VVHT will allow us to simulate a digital hydraulic transmission while allowing us to easily alter the available transmission ratios in software.

Moving forward, this enabling technology can be further validated in several ways. We need to more carefully examine the mechanical trade-offs we make by abandoning motors. To make the transition to steering by switching a digital hydraulic transmission, we need to address the hybrid control problem introduced by the discretization of selectable transmission ratios. In parallel with the work presented here, we are already approaching the dynamic modeling of digital hydraulic transmissions to capture effects like compliance and their effects on switching, building on [18].

We are additionally taking a clinical approach in collaboration with a sister lab, evaluating self-powered rehabilitation. While self-powered bimanual therapy is largely untested, it may hold promise along the same lines as constraint induced movement therapy [30] by encouraging exercise of the affected arm; rather than constraining the healthy arm completely, selective constraints force the healthy arm to work harder if the affected arm is slacking. Our preliminary work on self-powered teleoperation in able-bodied subjects has shown promise in reducing motor slacking [31], and further testing will be enabled by the technology presented here.

We have laid the theoretical groundwork for analysis and control of hydraulic joint constraints in this paper. We are hopeful that programmable body-powered wearable rehabilitation technology will enable new therapeutic paradigms that improve outcomes for those who have suffered a stroke.

Acknowledgments

Thanks to Mhairi Maclean for her work on developing the hydraulic elbow-elbow exoskeleton in Fig. 1. This work was supported by the National Institute of Biomedical Imaging and Bioengineering of the National Institutes of Health, Grant No. R01EB019834, and by the National Science Foundation Graduate Research Fellowship Program under Grant No. DGE1256260. Any opinions, findings, and conclusions or recommendations expressed in this material are those of the authors and do not necessarily reflect the views of the National Science Foundation or NIH.

References

1. Aisen ML, Krebs HI, et al. The Effect of Robot-Assisted Therapy and Rehabilitative Training on Motor Recovery Following Stroke. Archives of Neurology. 54:443–446.1997; [PubMed: 9109746]
2. Patton JL, Stoykov ME, et al. Evaluation of robotic training forces that either enhance or reduce error in chronic hemiparetic stroke survivors. Experimental Brain Research. 168:368–383.2006; [PubMed: 16249912]
3. Lam T, Wirz M, et al. Swing Phase Resistance Enhances Flexor Muscle Activity During Treadmill Locomotion in Incomplete Spinal Cord Injury. Neurorehabilitation and Neural Repair. 22(5):438–446.2008; [PubMed: 18780879]
4. Marchal-Crespo L, Reinkensmeyer DJ. Review of control strategies for robotic movement training after neurologic injury. Journal of neuroengineering and rehabilitation. 6(20):1–15.2009; [PubMed: 19154570]
5. Hesse S, Schmidt H, et al. Upper and lower extremity robotic devices for rehabilitation and for studying motor control. Current opinion in neurology. 16(6):705–710.2003; [PubMed: 14624080]
6. Peshkin MA, Colgate JE, et al. Cobot Architecture. IEEE Transactions on Robotics and Automation. 17(4):377–390.2001;
7. Jabre, L; McGrew, R; , et al. An assistive cobot for aid in self care activities; IFAC Conference on Mechatronic Systems; 2002. 1–6.
8. Pan, P; Lynch, KM; , et al. Human interaction with passive assistive robots; Proceedings of the 2005 IEEE 9th International Conference on Rehabilitation Robotics; 2005. 264–268.
9. Bosscher P, LaFay E. Haptic cobot exoskeleton: Concepts and mechanism design. Proceedings of the ASME Design Engineering Technical Conference. 20062006; :1–10.
10. Li, X, Chua, JY, Moore, CA. ASME International Mechanical Engineering Congress and Exposition. Orlando: 2005. Design and Control of a 3-D Wearable Cobot; 1–7.
11. Nordin N, Xie SQ, Wünsche B. Assessment of movement quality in robot- assisted upper limb rehabilitation after stroke : a review. Journal of neuroengineering and rehabilitation. 11(137):1–23.2014; [PubMed: 24393611]
12. Rose DK, Winstein CJ. Bimanual Training After Stroke: Are Two Hands Better Than One? Topics in Stroke Rehabilitation. 11(4):20–30.2004; [PubMed: 15592987]
13. Sleimen-Malkoun R, Temprado J-J, et al. Bimanual training in stroke: How do coupling and symmetry-breaking matter? BMC neurology. 11(11):1–9.2011; [PubMed: 21208452]
14. Faulring EL, Colgate JE, Peshkin MA. The Cobotic Hand Controller: Design, Control and Performance of a Novel Haptic Display. The International Journal of Robotics Research. 25(11): 1099–1119.2006;
15. Linjama, M, Huhtala, K. Workshop on Digital Fluid Power. Tampere; 2010. Digital hydraulic power management system - towards lossless hydraulics; 5–22.
16. Linjama, M, Laamanen, A, Vilenius, M. Scandinavian International Conference on Fluid Power. Tampere; 2003. IS IT TIME FOR DIGITAL HYDRAULICS?.
17. Linjama, M. DIGITAL FLUID POWER - STATE OF THE ART. Twelfth Scandinavian International Conference on Fluid Power; May 2011; Tampere; 2011.
18. Gan, Z, Fry, K. , et al. Intelligent Robots and Systems, IEEE/RSJ International Conference on. Hamburg: IEEE; 2015. A Novel Variable Transmission with Digital Hydraulics; 5838–5843.
19. Gillespie RB, Colgate JE, Peshkin MA. A General Framework for Cobot Control. IEEE Transactions on Robotics and Automation. 17(4):391–401.2001;
20. Achten, P, Fu, Z, Vael, G. The Fifth Scandinavian International Conference on Fluid Power. Linkoping; Sweden: 1997. Transforming future hydraulics: a new design of a hydraulic transformer; 1–24.
21. Karnopp, DC, Margolis, DL, Rosenberg, RC. System Dynamics: Modeling, Simulation, and Control of Mechatronic Systems. 5. Vol. ch. 7.5. Hoboken: Wiley; 2012. Multiport Transformers; 359–364.

22. Beer RF, Given JD, Dewald JPA. Task-dependent weakness at the elbow in patients with hemiparesis. Archives of Physical Medicine and Rehabilitation. 80(7):766–772.1999; [PubMed: 10414760]
23. Whitney, JP; Glisson, MF; , et al. A Low-Friction Passive Fluid Transmission and Fluid-Tendon Soft Actuator; IEEE/RSJ International Conference on Intelligent Robots and Systems; 2014. 2801–2808.
24. Gillespie RB, Moore CA, et al. Kinematic Creep in a Continuously Variable Transmission: Traction Drive Mechanics for Cobots. Journal of Mechanical Design. 124(4):713.2002;
25. Hodgson AJ, Emrich R. Control of Minimally Constrained Cobots. Journal of Robotic Systems. 19(7):299–314.2002;
26. Coulter RC. Implementation of the Pure Pursuit Path Tracking Algorithm. Carnegie-Mellon Univ. Robotics Inst, Pittsburgh, Tech. Rep. 1992
27. Colgate JE. Robust impedance shaping telemanipulation. Robotics and Automation, IEEE Transactions on. 9(4):374–384.1993;
28. Goldfarb, M. IEEE International Conference on Robotics and Automation. Vol. 2. Leuven; May, 1998 Dimensional analysis and selective distortion in scaled bilateral telemanipulation; 1609–1614.
29. Hashtrudi-Zaad K. Analysis of Control Architectures for Teleoperation Systems with Impedance/Admittance Master and Slave Manipulators. The International Journal of Robotics Research. 20(6):419–445.2001;
30. Taub E, Uswatte G, Pidikiti R. Constraint-induced movement therapy: A new family of techniques with broad application to physical rehabilitation–a clinical review. Journal of Rehabilitation Research and Development. 36(3):237–251.1999; [PubMed: 10659807]
31. Washabaugh, EP, , IVTreadway, E. , et al. 2016 Neuroscience Meeting Planner, Program No. 533.12. San Diego, CA: 2016. Self-powered robots to minimize motor slacking during rehabilitation.

Biographies

Emma Treadway is a Ph.D. Candidate in Mechanical Engineering at the University of Michigan, Ann Arbor. She received her M.S.E. in Mechanical Engineering from the University of Michigan in 2017 and her B.S. in Engineering Science from Trinity University in 2011. Her research interests include human-robot interaction, rehabilitation robotics, prosthetics, and haptics.

Zhenyu Gan is a Ph.D. Candidate of Mechanical Engineering at the University of Michigan, Ann Arbor. He received his M.Sc. in Mechanical Engineering from the University of Michigan and his B.S. in Mechanical Engineering from the Shandong University. His interests include multibody dynamics, gait pattern analysis of bipedal and quadrupedal locomotion, and control of body-powered exoskeletons.

C. David Remy is Assistant Professor of Mechanical Engineering at the University of Michigan, Ann Arbor. He received his Ph.D. from ETH Zurich, and holds both a M.Sc. in Mechanical Engineering from the University of Wisconsin and a Diploma in Engineering Cybernetics from the University of Stuttgart. Dr. Remy is the head of the Robotics and Motion Laboratory (ram-lab.engin.umich.edu). His research interests include the design, simulation, and control of legged robots, exoskeletons, and other nonlinear systems. Drawing inspiration from biology and biomechanics, he is particularly interested in the effects and exploitation of natural dynamic motions, the role of different gaits, and the possibility of force/torque controllable systems; both in conceptual models and in hardware realizations.

R. Brent Gillespie received the BS degree in mechanical engineering from the University of California, Davis, in 1986, the M degree in piano performance from the San Francisco Conservatory of Music in 1989, and the MS and PhD degrees in mechanical engineering from Stanford University, Stanford, CA, in 1992 and 1996, respectively. He is currently with the Department of Mechanical Engineering, University of Michigan, Ann Arbor. His current research interests include haptic interface and teleoperator control, human motor control, and robot-assisted rehabilitation after neurological injury. He is a member of the IEEE.

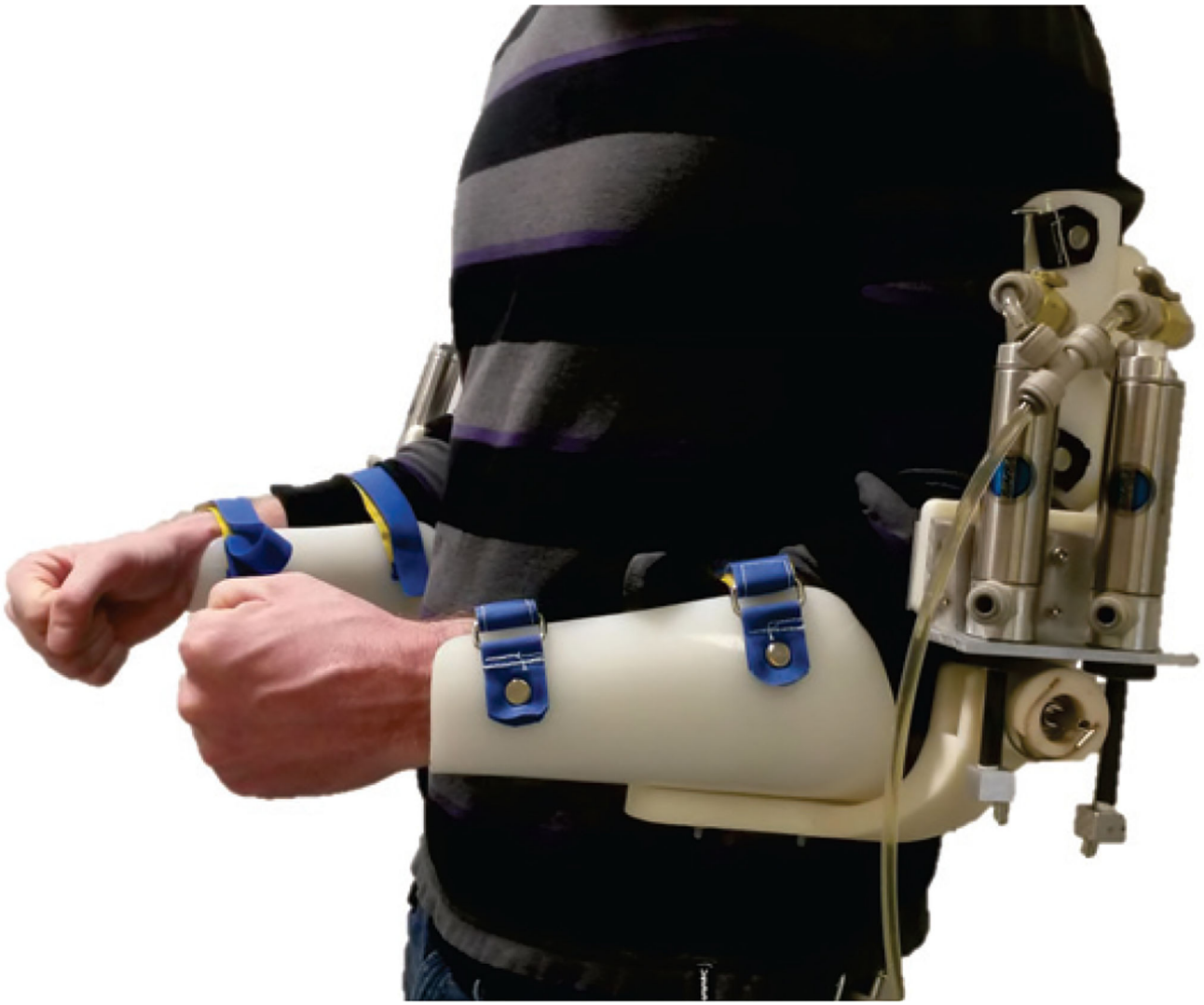

Fig. 1.
Prototype elbow—elbow hydraulic cobot capable of two transmission ratios: +1:1 and −1:1.

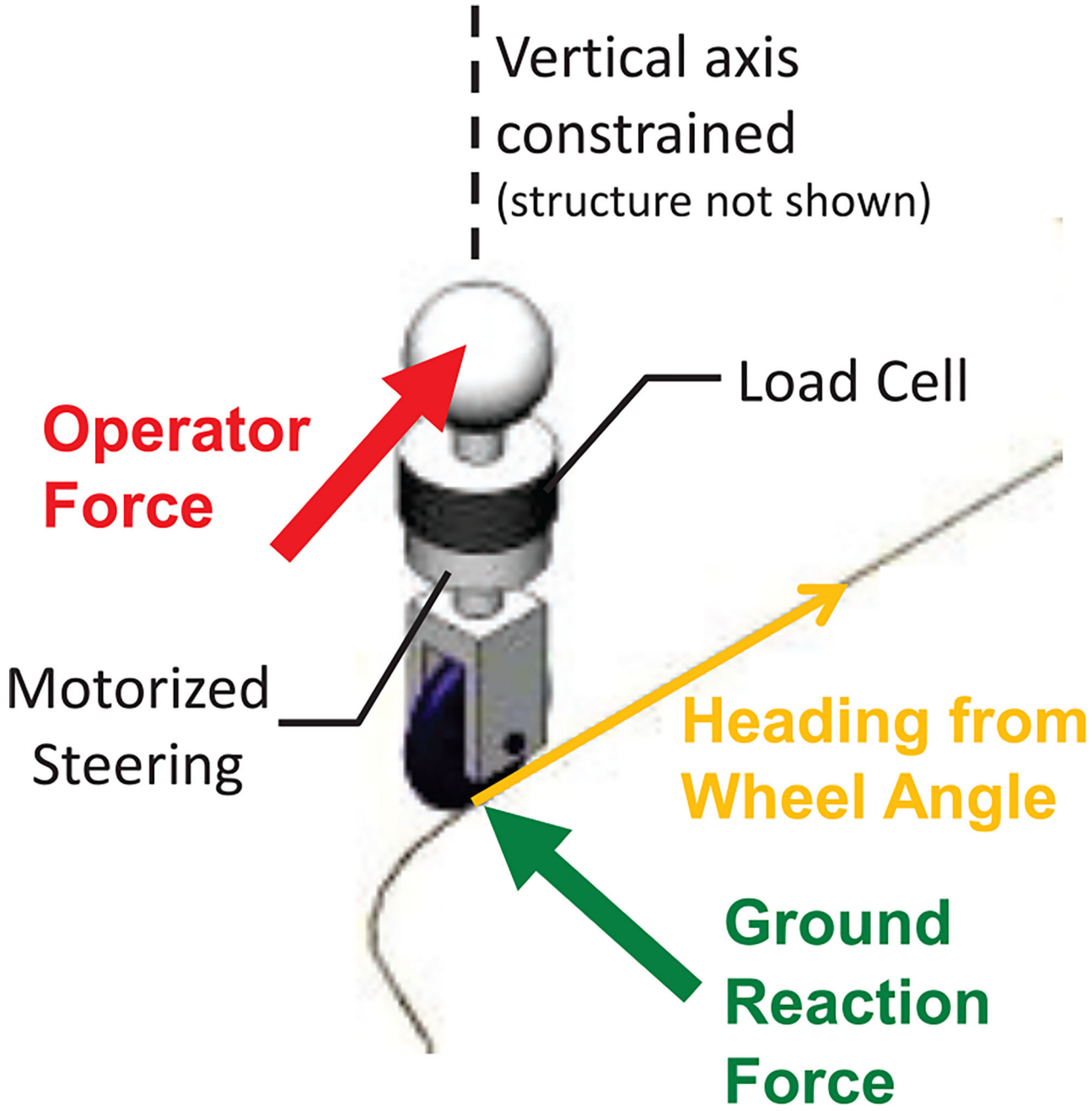

Fig. 2.
Traditional cobots use wheels or rolling-contact CVTs to impose constraints, and compensate for measured interaction forces to display free space.

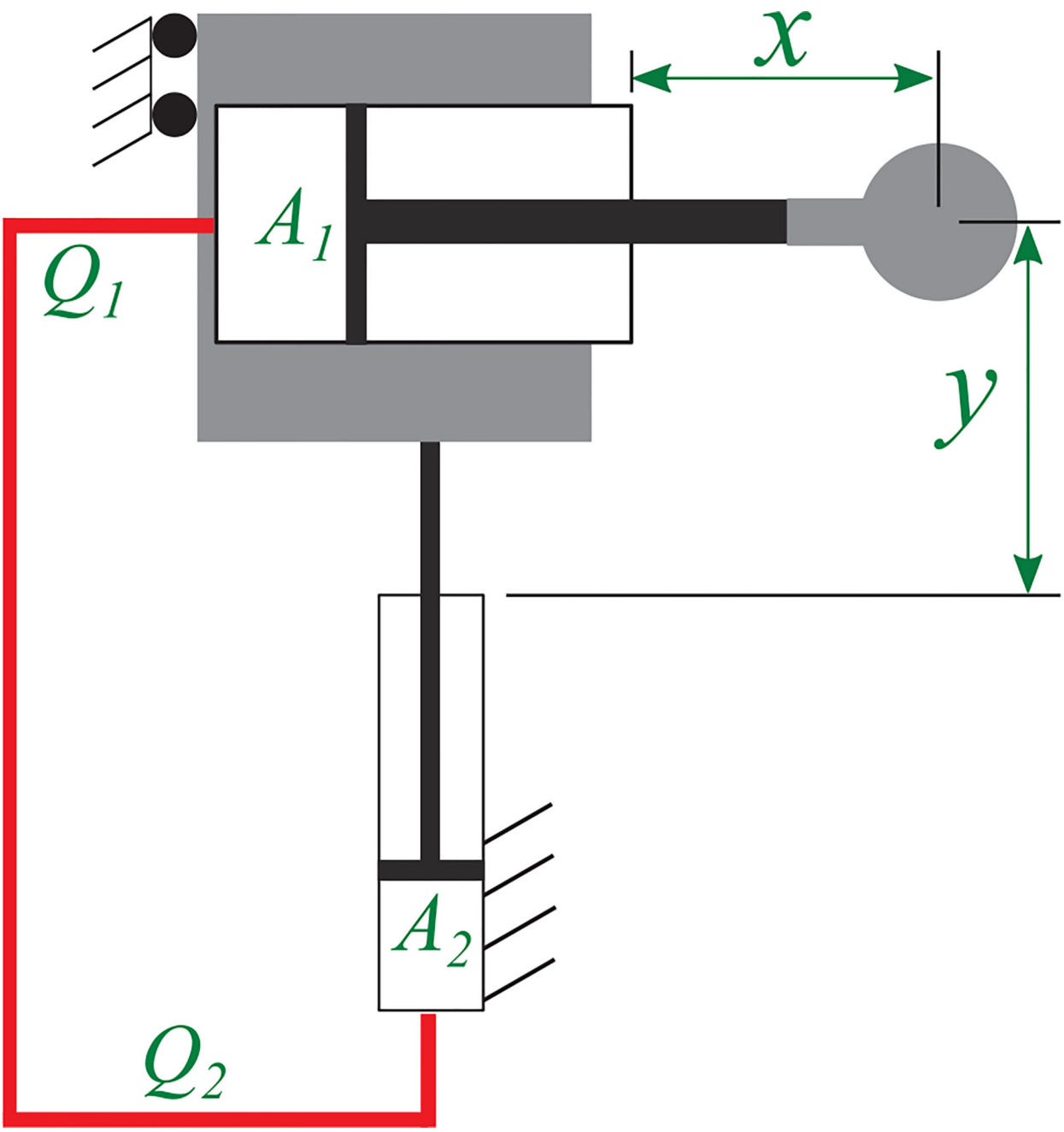

Fig. 3.

A Cartesian hydraulic constraint machine. The transmission places a constraint on the relative motion $\dot{y}/\dot{x}$ of the end effector (pictured as a gray knob).

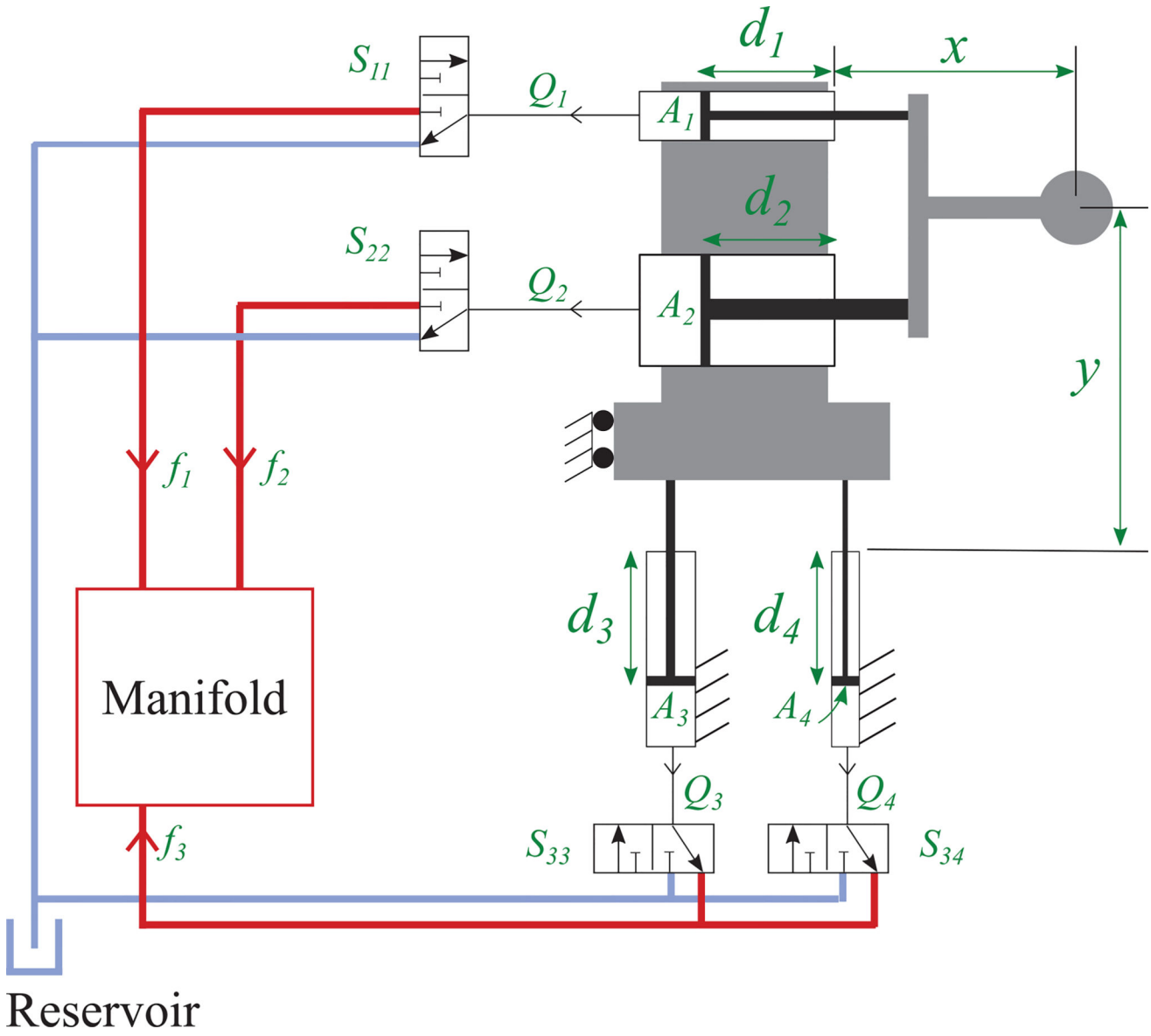

Fig. 4.

An example of a simple two-joint digital hydraulic circuit. Valves allow each cylinder to be connected either to the reservoir (blue) or to a common hydraulic manifold (red). The transmission ratio is based on the relative face areas of the cylinders connected to the common manifold on each joint. The transmission places a constraint on the relative motion $\dot{y}/\dot{x}$ of the end effector (pictured as a gray knob).

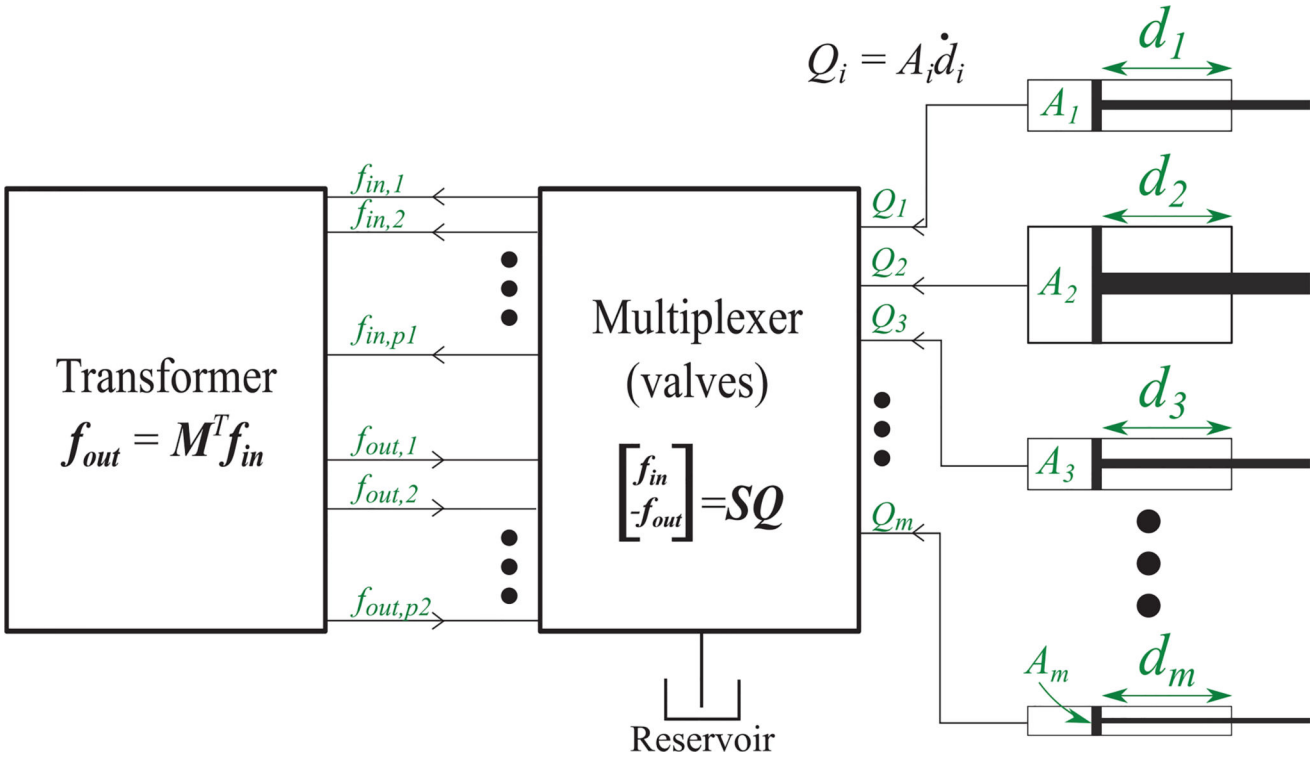

Fig. 5.

Introducing programmability to the relationship between flows, with the multiplexer valves S and the transformer relationship M.

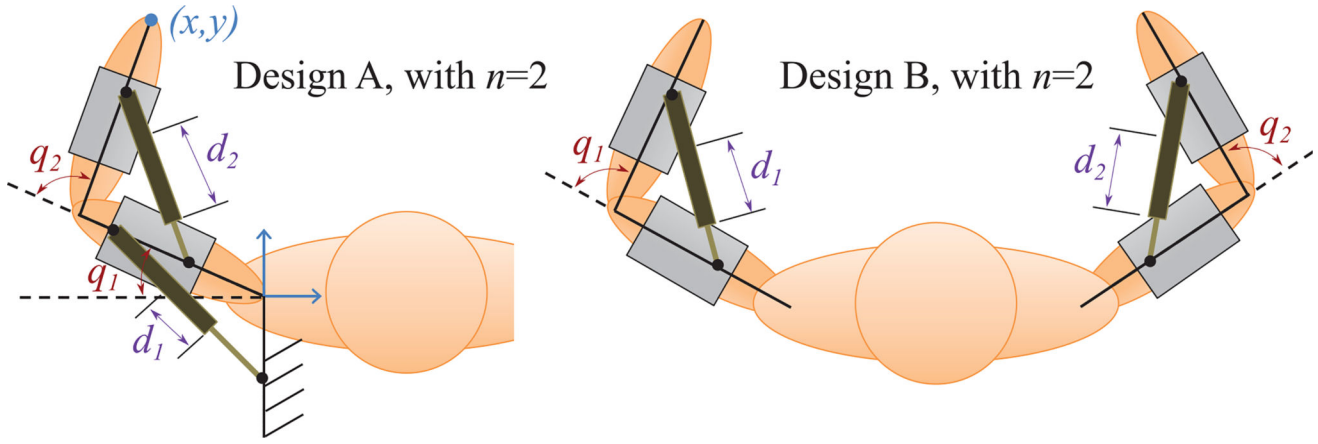

Fig. 6.

A wearable constraint device (left) spanning the successive shoulder and elbow joints on a single limb to form a kinematic chain (design A), and (right) spanning the elbow joints on two different limbs (design B).

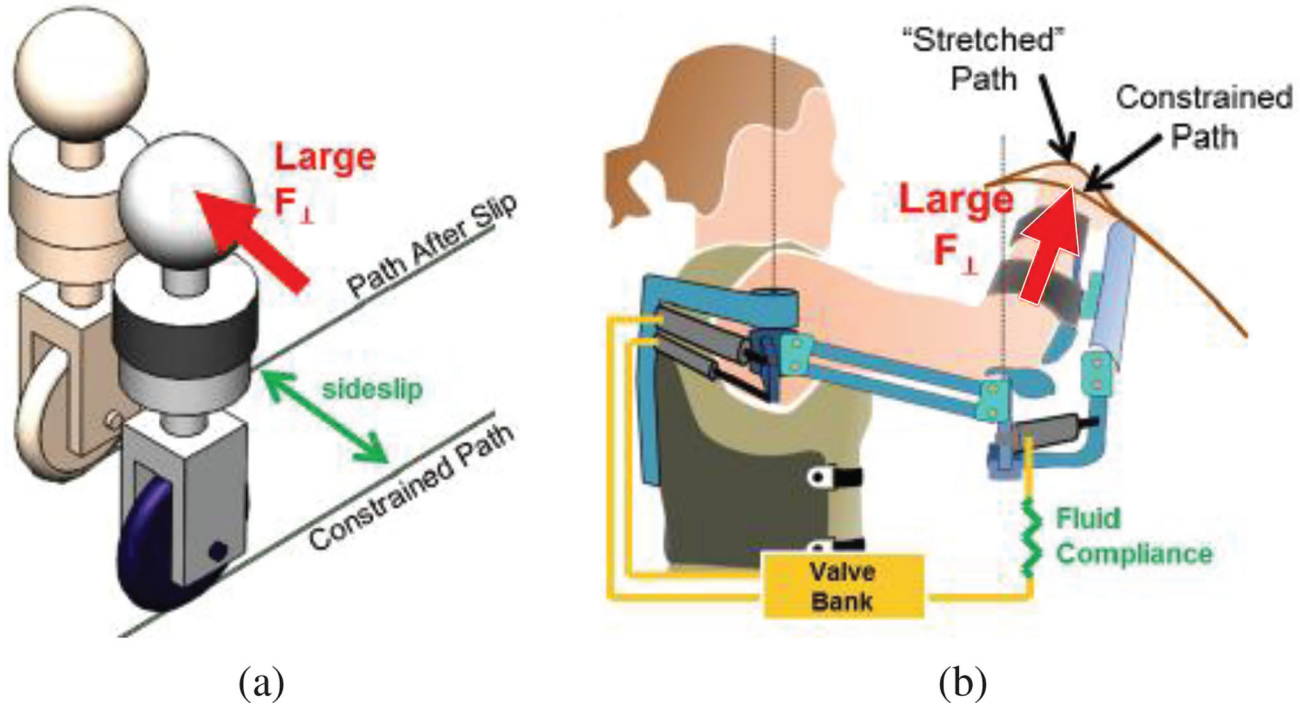

Fig. 7.

(a) The ability to support loads $F_{\perp}$ perpendicular to the rolling direction in rolling-contact CVTs is limited by the possibility of gross slip and frustrated by the likelihood of sideslip, making mechanical design of wearable cobots virtually untenable. (b) A Digital Fluid Transmission, using valves to select from a set of available transmission ratios, can support large loads without slip. The fluid's bulk modulus instead results in compressibility, which results in a return to the desired path when $F_{\perp}$ is removed.

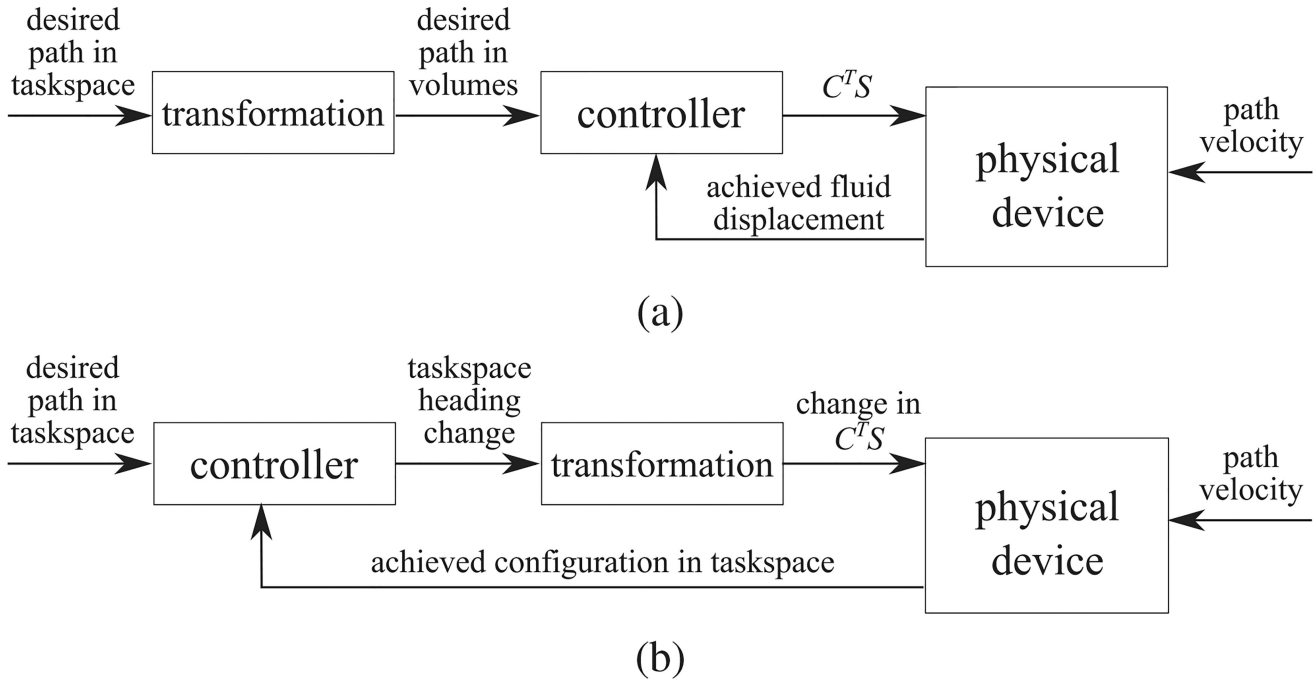

Fig. 8.

Options for flow constraints based on desired motion in taskspace. (a) Paths are transformed to volume relationships, and control computed at the flow level, or (b) taskspace headings are computed and transformed to $\mathbf{C}^T\mathbf{S}$.

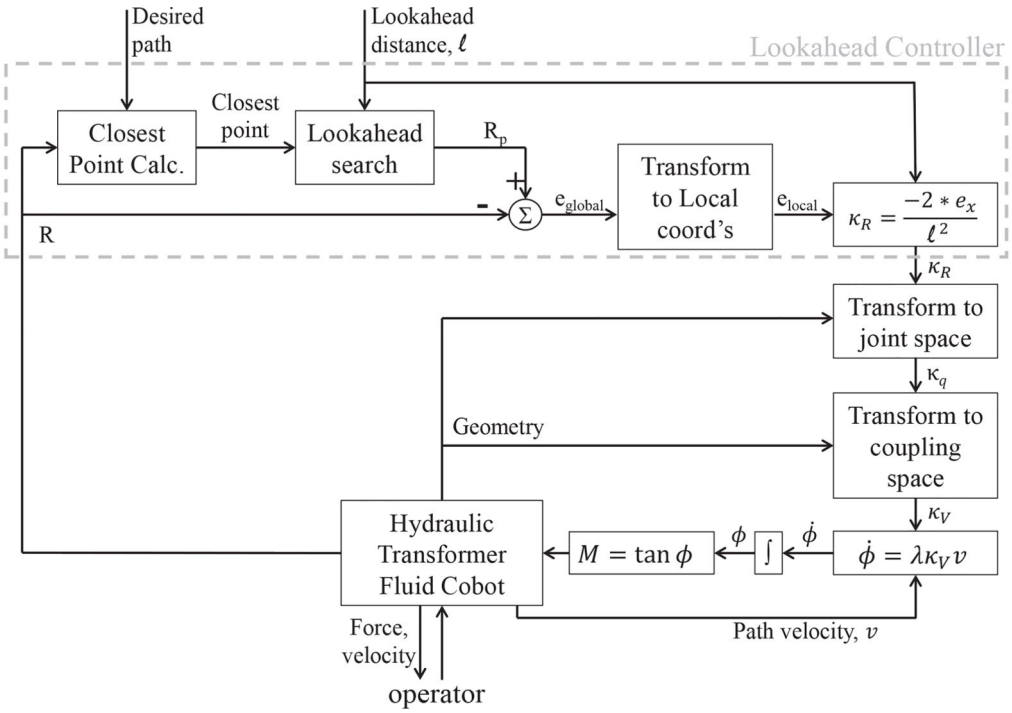

(a) Required path curvature to reach the desired point at the lookahead distance is calculated, and then converted to coupling space, where the resulting heading change is enforced through the transmission ratio.

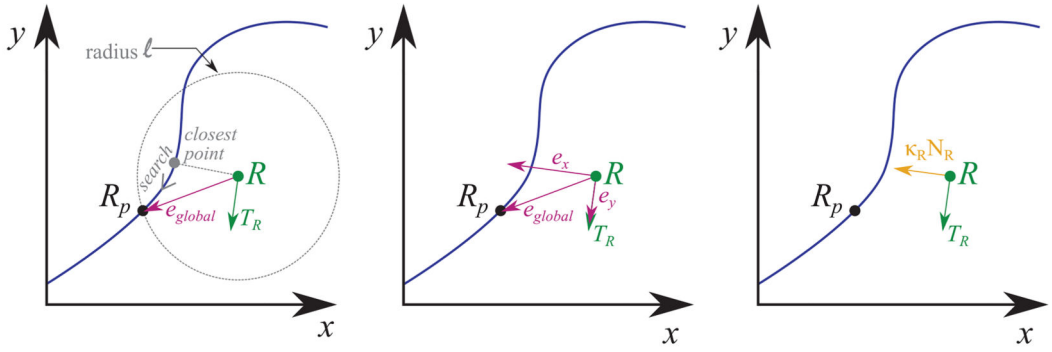

(b) Illustration of lookahead curvature calculation steps.

Fig. 9.

Lookahead steering controller for a cobot in configuration R moving in the direction of heading T_R, with a desired path defined in taskspace.

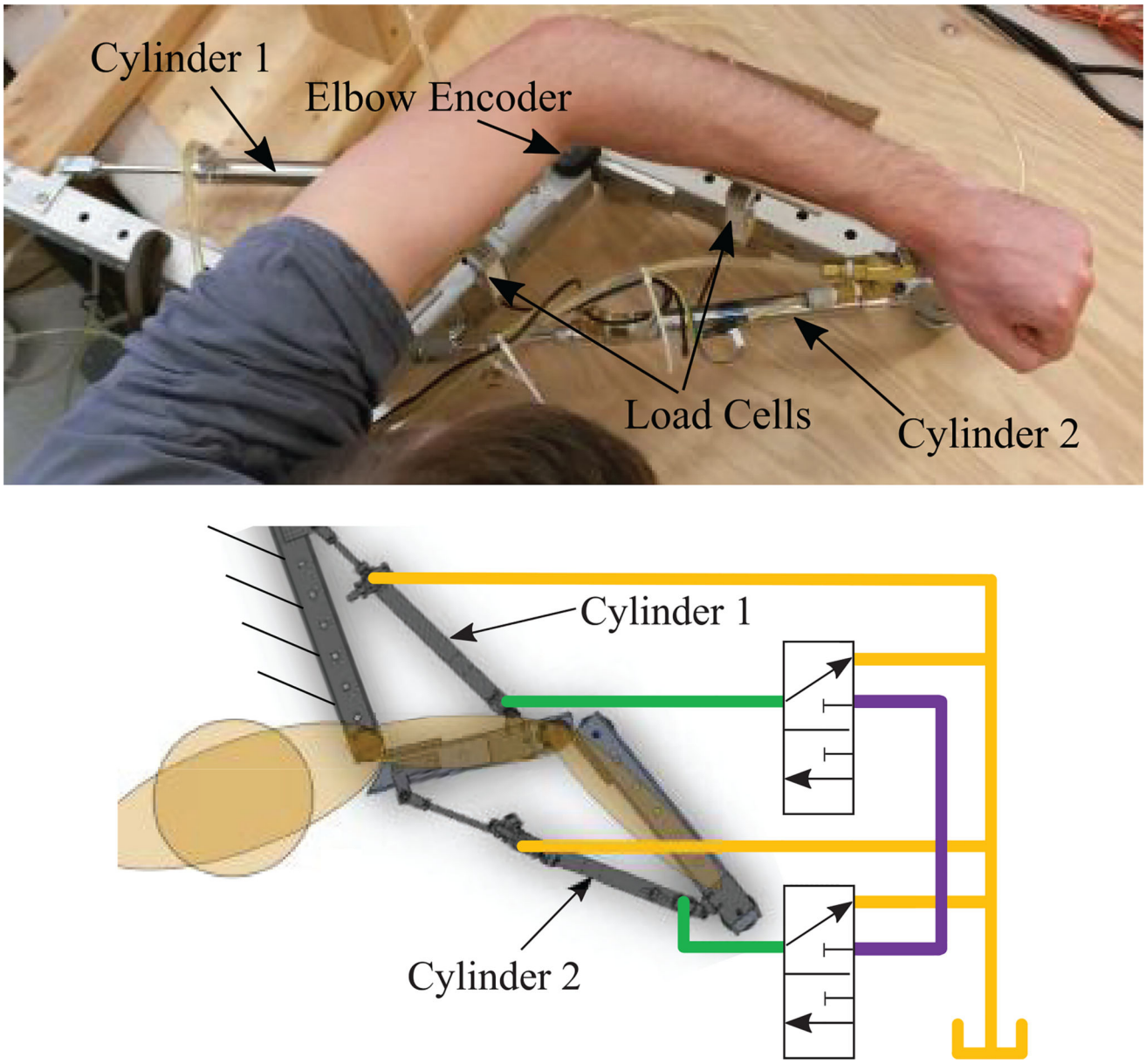

Fig. 10.

Simple two-joint shoulder-elbow exoskeleton prototype, pictured for $M = 1$. Valves allow either a −1:1 transmission ratio to be imposed between the two cylinders through the manifold (purple), free motion by opening both cylinders to the reservoir (yellow), or locked position by opening a single cylinder to the reservoir while the other is connected to the common manifold. Load cells are used to measure interaction forces, but no active force control is needed.

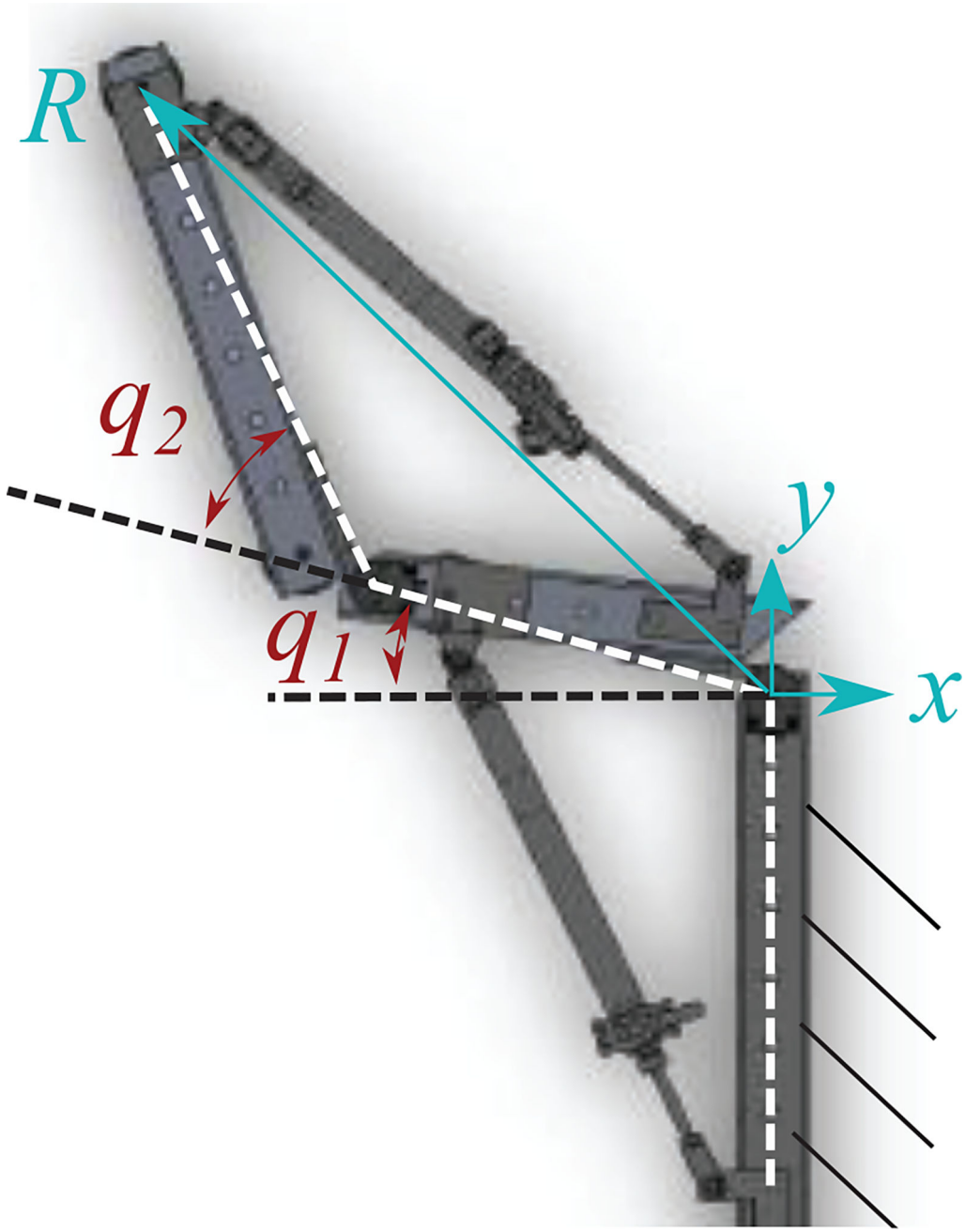

Fig. 11.
Definition of joint-and taskspace variables for elbow-shoulder prototype.

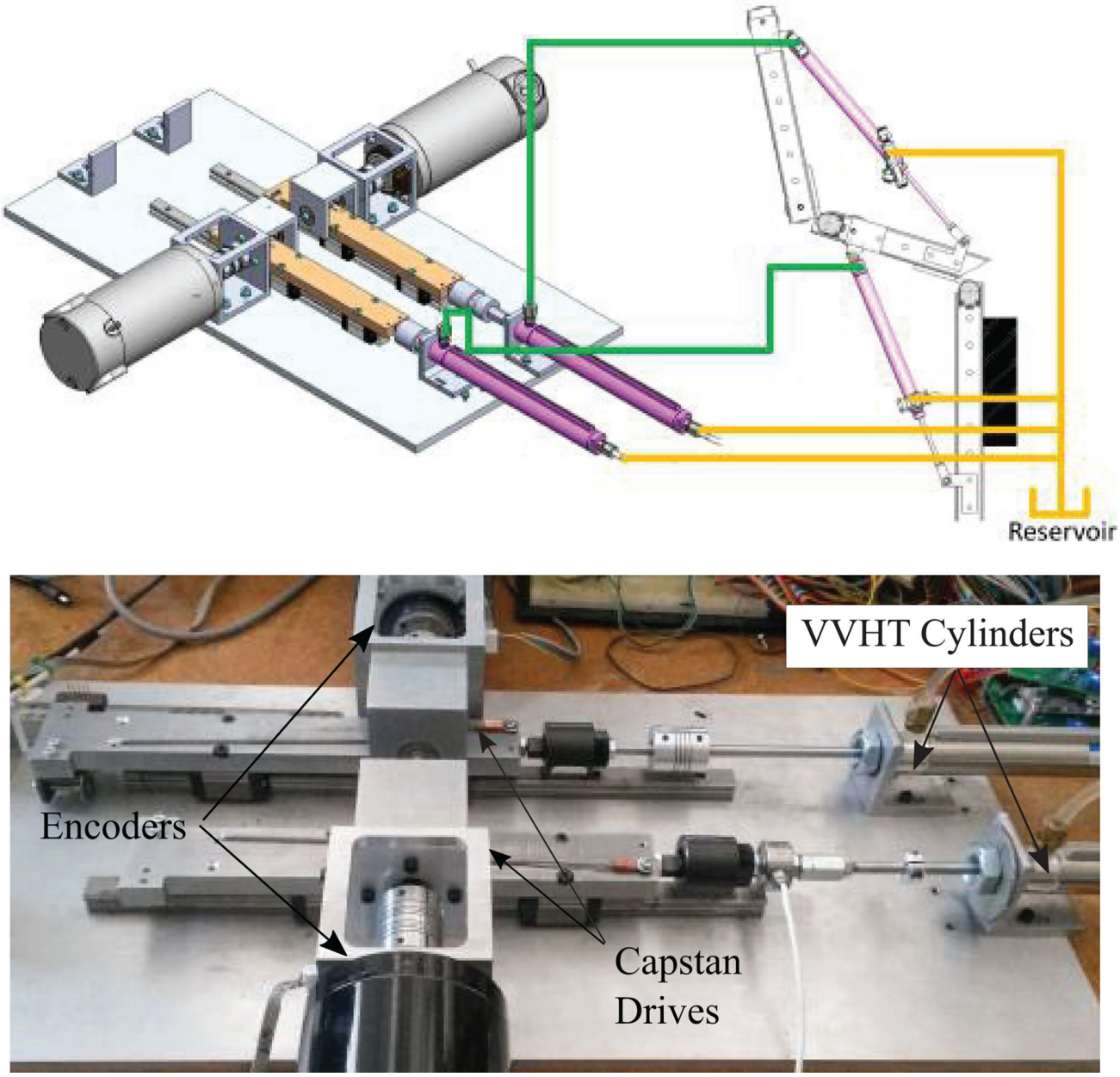

Fig. 12.

VVHT and planar elbow-shoulder prototype. The prototype exoskeleton used is the same as pictured earlier. Encoders and load cells are used to implement a variable transmission ratio between the two cylinders when **S** = **I** by controlling the motors' relative torques and positions.

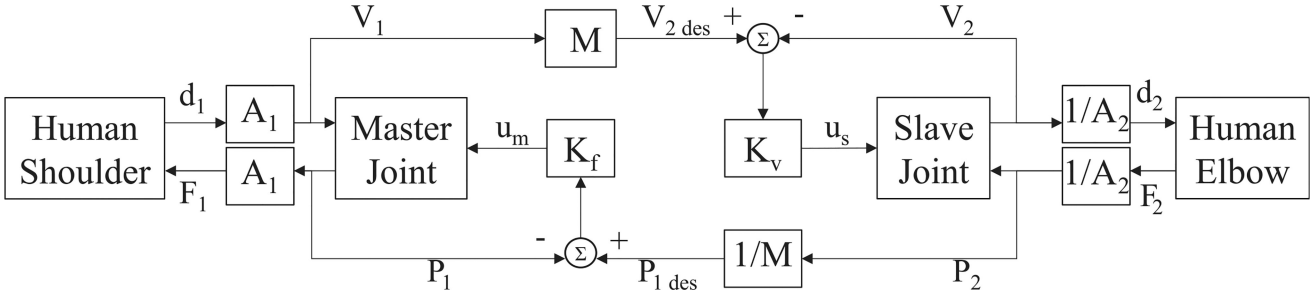

Fig. 13.

2-Channel force-position teleoperator control scheme to simulate a CVT with two separate motion axes. A hydraulic transformer would naturally impose relationships on pressures (P_1, P_2) and volumes/flows (V_1, V_2); here, however, since $A_1 = A_2$, we were able to directly impose the relationships between displacements and joint torques.

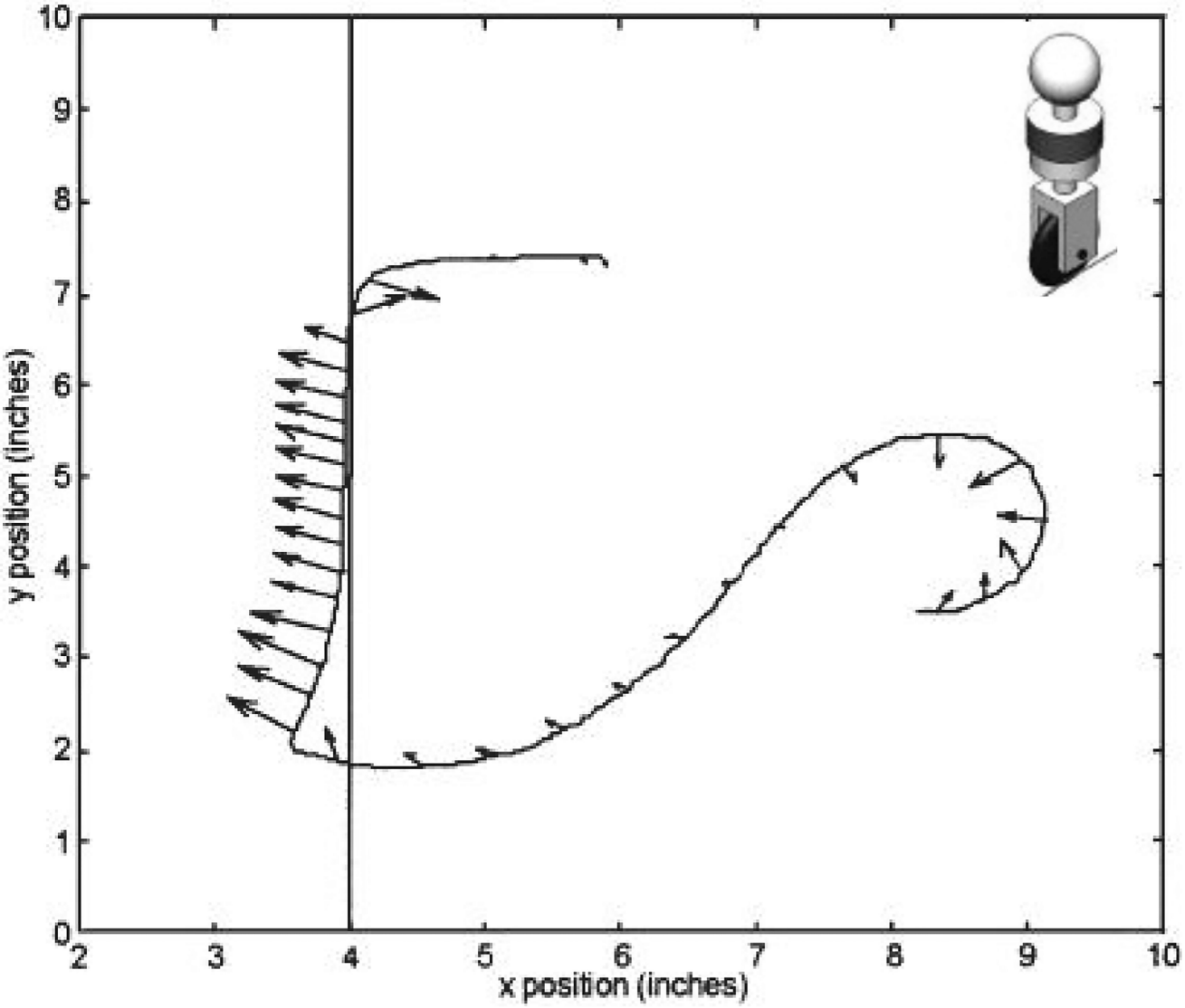

Fig. 14.

Free space and constraint rendering with the unicycle cobot. User forces are given as vectors on top of the solid curve representing the trajectory. Figure reproduced from [6] with permission.

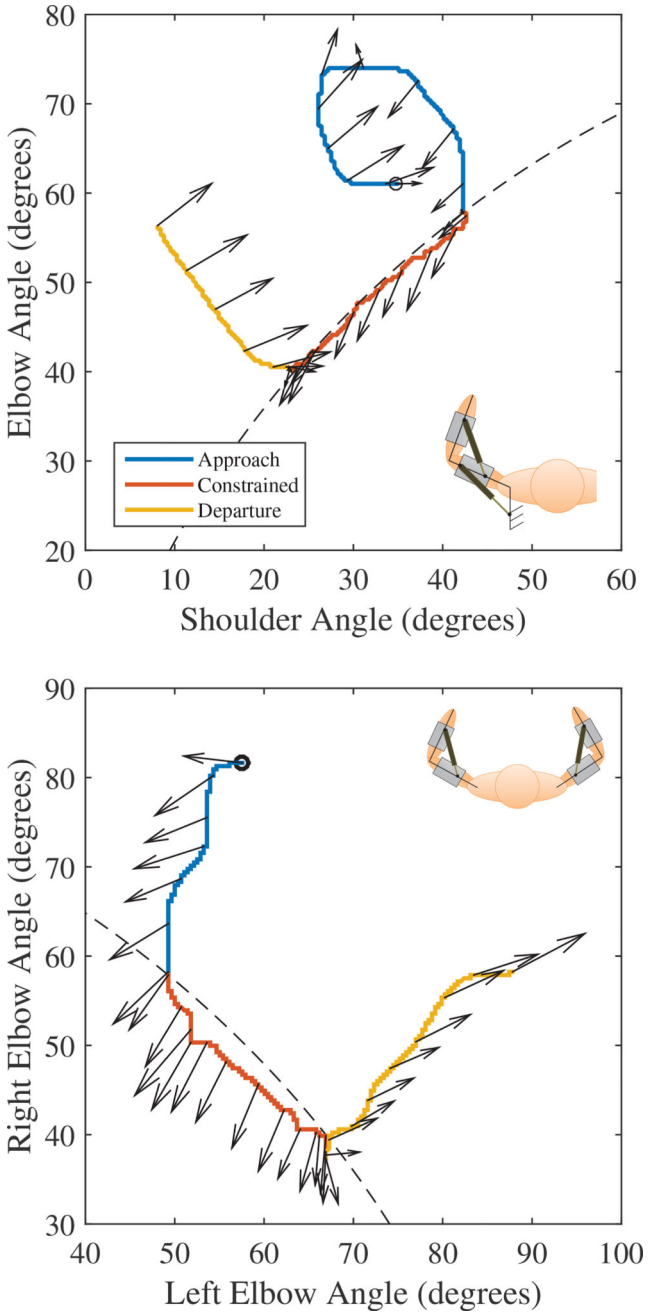

Fig. 15.

Free space and constraint for digital hydraulic shoulder-elbow (top) and elbow-elbow (bottom) exoskeletons.

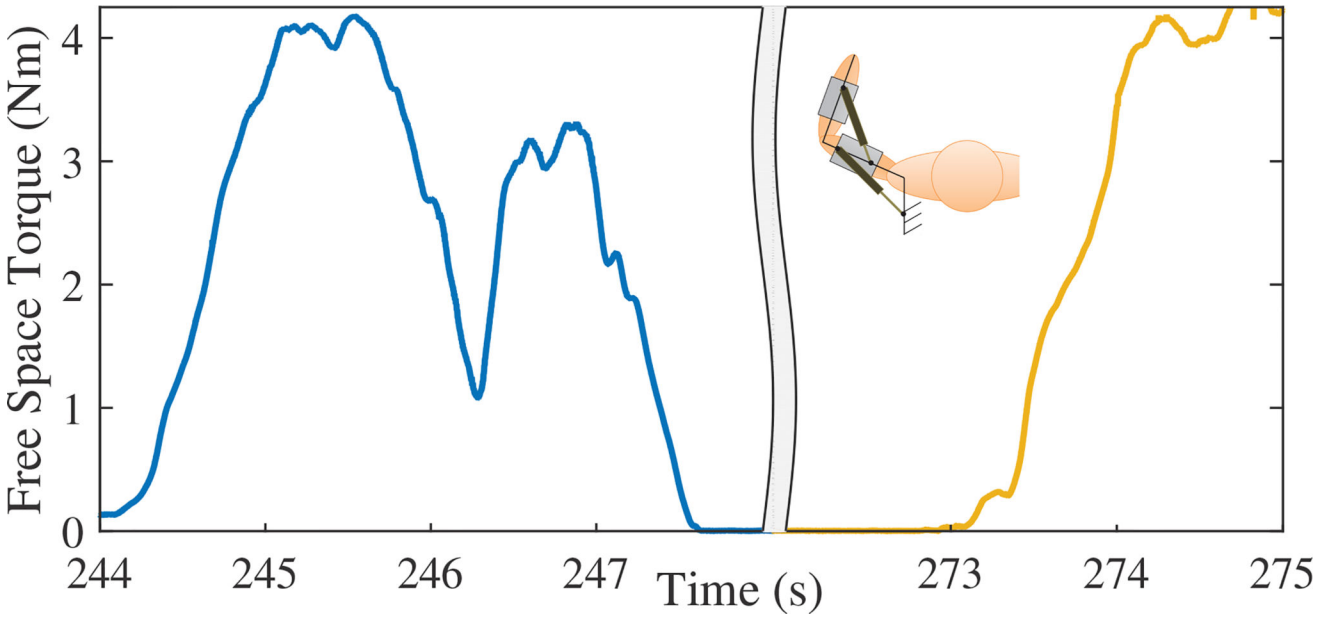

Fig. 16.

Measured free-space force magnitudes during approach and departure from constraint for the digital hydraulic shoulder-elbow exoskeleton. Forces are the same as shown with overlay arrows in the top pane of Fig. 15

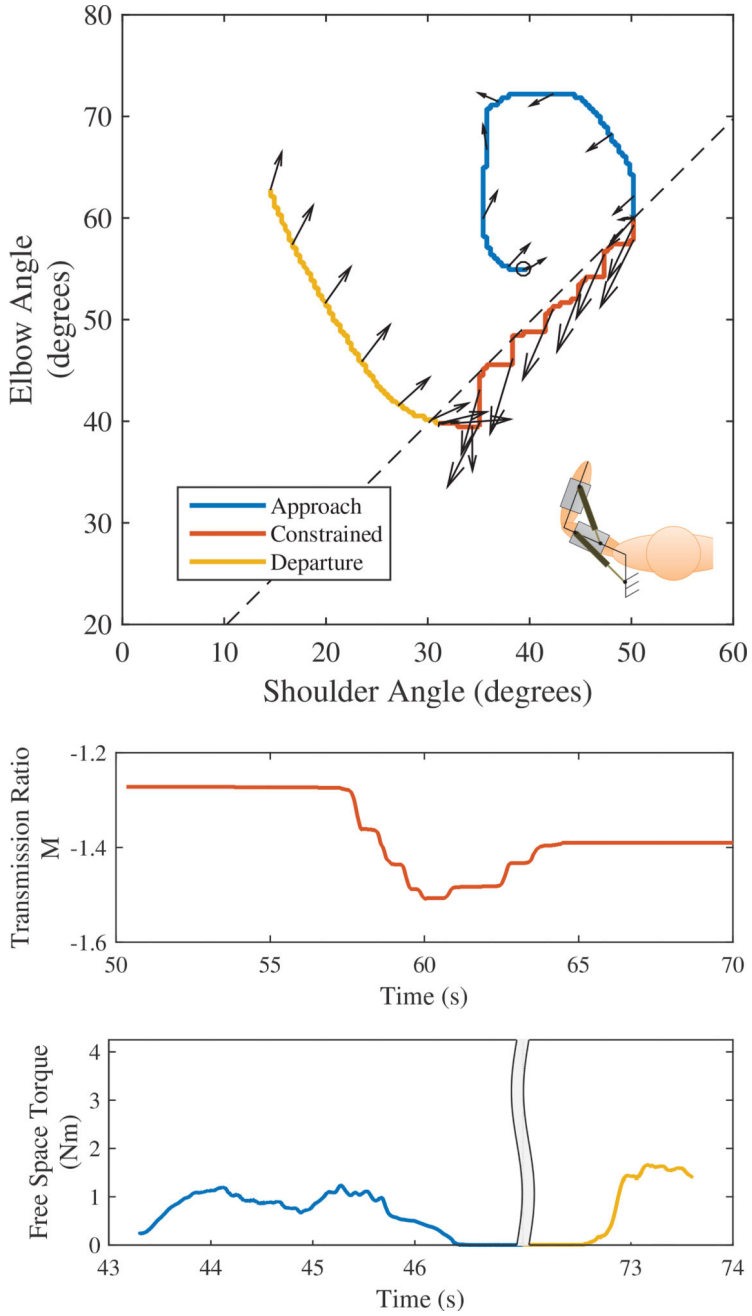

Fig. 17.

(Top) Free space and constraint for exoskeleton with VVHT. User forces are given as vectors on top of the solid curve representing the trajectory. (Middle) Transmission ratio calculated by the lookahead controller and (bottom) user forces measured during free space motion approaching and departing from the constraint.

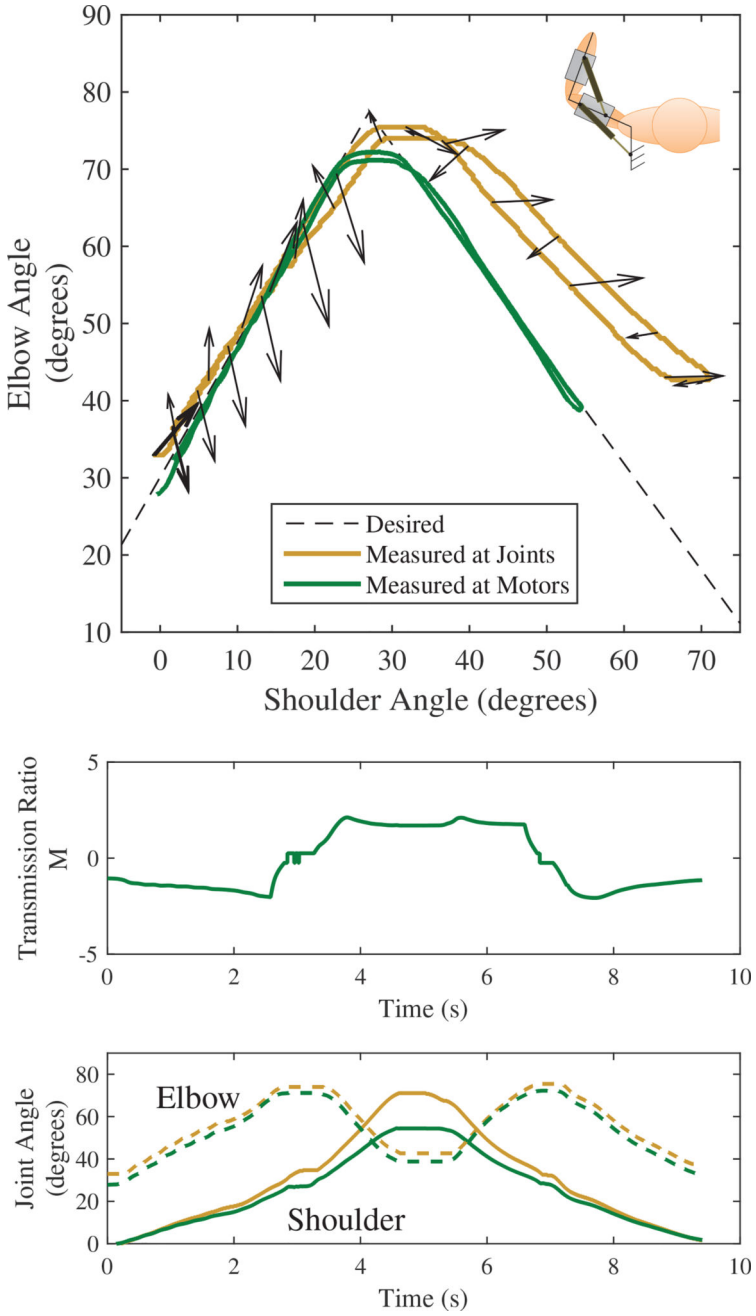

Fig. 18.

(Top) Free space and constraint for hydraulic virtual transmission imposing a more complex path. User forces are given as vectors on top of the solid curve representing the trajectory. (Middle) Transmission ratio calculated by the lookahead controller and (bottom) joint trajectories in time throughout the motion. For all plots, quantities measured/imposed at the motors are shown in green, and quantities at the exoskeleton joints are gold.